NATIONAL ADVISORY COMMITTEE
FOR AERONAUTICS

TECHNICAL NOTE 3983

EFFECT OF STANDING TRANSVERSE ACOUSTIC OSCILLATIONS

ON FUEL-OXIDANT MIXING IN CYLINDRICAL

COMBUSTION CHAMBERS

By William R. Mickelsen

Lewis Flight Propulsion Laboratory
Cleveland, Ohio

NACA

Washington
May 1957

TABLE OF CONTENTS

NATIONAL ADVISORY COMMITTEE FOR AERONAUTICS

─────────

TECHNICAL NOTE 3983

─────────

EFFECT OF STANDING TRANSVERSE ACOUSTIC OSCILLATIONS ON FUEL-OXIDANT

MIXING IN CYLINDRICAL COMBUSTION CHAMBERS

By William R. Mickelsen

SUMMARY

The effect of acoustic oscillations on fuel-oxidant mixing is ana-
lyzed for acoustic conditions commonly found in screeching and screaming
combustors. Transverse acoustic fields in cylindrical ducts are described
in terms of pressure fluctuation, particle velocity, and oscillation
frequency. The effect of such acoustic fields on the fuel-oxidant mixing
downstream from point sources of injection is treated theoretically to
obtain expressions relating the fuel-oxidant ratio to the parameters of
the stream and the acoustic field. Numerical solutions of these relations
are made to illustrate the effect of sound-pressure level, oscillation
frequency, stream velocity, and turbulence level. The results of this
analysis show that, for moderate screech or scream levels, the fuel-
oxidant mixing wake is given a transverse oscillatory motion of consider-
able magnitude and that the fuel-oxidant ratio undergoes large cyclic
fluctuations which are in phase with the pressure fluctuations of the
acoustic field. A number of possible mechanisms contributing to screech
and scream in various combustor configurations are proposed, and methods
for their control are suggested.

INTRODUCTION

The effect of acoustic fields on vapor mixing is of interest to the
combustion problem in screeching or screaming combustors. If the acoustic
oscillations change the fuel-air or fuel-oxidant ratio, the combustion
process will be directly affected. To illustrate the effect of acoustic
oscillations, an analysis has been made of vapor mixing in cylindrical
ducts under conditions usually found in screeching ramjets and after-
burners and in screaming rockets.

Acoustic oscillations in cylindrical chambers have three general
modes: longitudinal, radial, and tangential, as illustrated by the
following pressure fluctuation diagrams showing pressure fluctuation
contours at an instant in time:

Longitudinal   Radial   Tangential

(a)
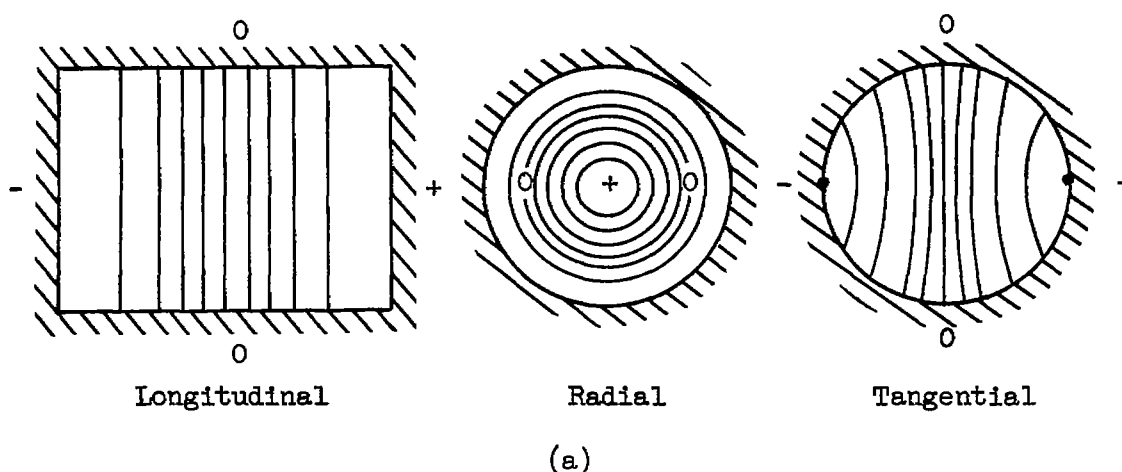
Pressure fluctuation maximums alternate in sign with time. The modes
shown are the fundamentals; higher modes exist for each type. As pointed
out in references 1 to 4, acoustic oscillations in ramjet combustors,
afterburners, and rockets may be any of these types, depending on a
number of aerodynamic and combustion factors.

The pressure fluctuations in each of the modes of oscillation give
rise to acoustic particle velocities which can affect the aerodynamic
mixing in a manner somewhat similar to that of turbulent velocity fluctua-
tions. This effect has been analyzed in reference 5, where it is shown
that the action of a transverse acoustic particle velocity produces a
sinusoidal-shaped deformation of the concentration pattern downstream
from a source of heat or mass. A typical deformed mixing wake at an
instant in time is shown in the following sketch:

(b)

4379
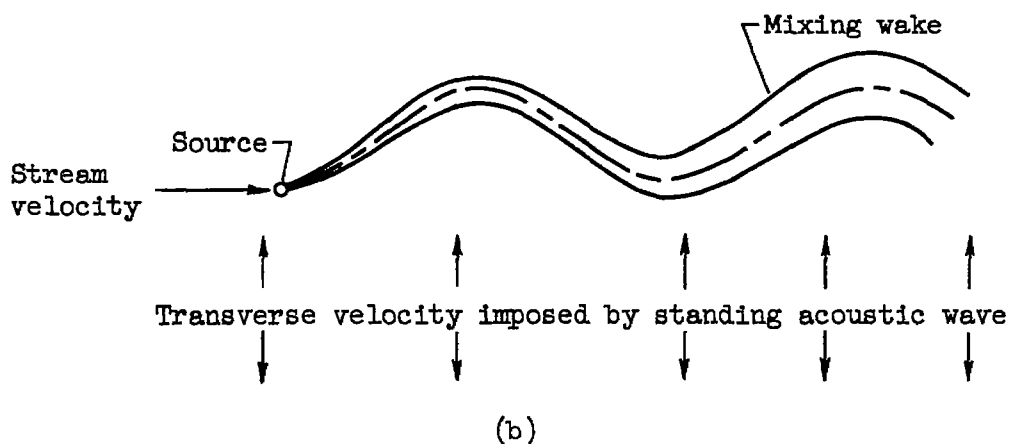
The analysis of reference 5 shows that, if the deformation is severe, the concentration of the heat or mass is changed considerably. In addition to the transverse motion of the wake, the shape and magnitude of the concentration profile at any axial station is shown to change with time. The deformation of the wake is shown to increase with particle velocity and, hence, with sound-pressure level. The pressure perturbations reported in references 2 and 4 are sufficiently large to produce transverse particle velocities of the same order as the stream velocity. Acoustic oscillations of these magnitudes can strongly affect the concentration level.

To illustrate the effect of transverse acoustic oscillations on fuel-air or fuel-oxidant mixing, the analysis in reference 5 is extended herein to a range of acoustic conditions which exist in jet-engine and rocket combustors. The acoustic field is described in terms of pressure fluctuation and particle velocity patterns and oscillation frequency. An idealized mixing model is used which consists of a point source of fuel vapor injected at a constant rate into a flowing, turbulent oxidant stream. Mixing equations are derived which define the fuel-oxidant ratio at any point in the field and at any time during the acoustic oscillation. The effect of tangential acoustic oscillations on the vapor mixing is shown to be a composite function of acoustic pressure and frequency, stream velocity, and turbulence. Each of these four variables is treated separately so that trends in fuel-oxidant ratio may be observed graphically.

In addition to the specific conclusions drawn from the results of this analysis, a discussion is included which offers mechanisms which might contribute to the driving of the acoustic oscillations and suggests methods for their control or elimination.

PROPERTIES OF THE ACOUSTIC FIELD

Experiment has indicated that screeching ramjet combustors and turbojet afterburners and screaming rocket combustion chambers have acoustic fields approximated by the closed-end cylinder case. With the cylinder closed at both ends, the transverse modes of oscillation are preserved throughout the length of the combustor. Departure from this uniformity of transverse modes is discussed later in this section. As a preliminary to the derivation of the fuel-oxidant mixing equations, the acoustic field in closed-end cylinders is described in terms of pressure fluctuations (sound pressure), particle velocity, and oscillation frequency for a range of gas conditions likely to be encountered in combustors.

Sound Pressure

The general solution of the wave equation for the pressure fluctuation is given in reference 6 (p. 398) and includes all possible modes (longitudinal, radial, and tangential) and their harmonics. The class of oscillations of interest to the present analysis is the tangential modes called the pure standing, pure spinning, and combined standing and spinning. The pressure patterns of these three tangential modes are shown in sketch (c):

| First pure-
standing mode | First pure-
spinning mode | Combination
spinning-standing |
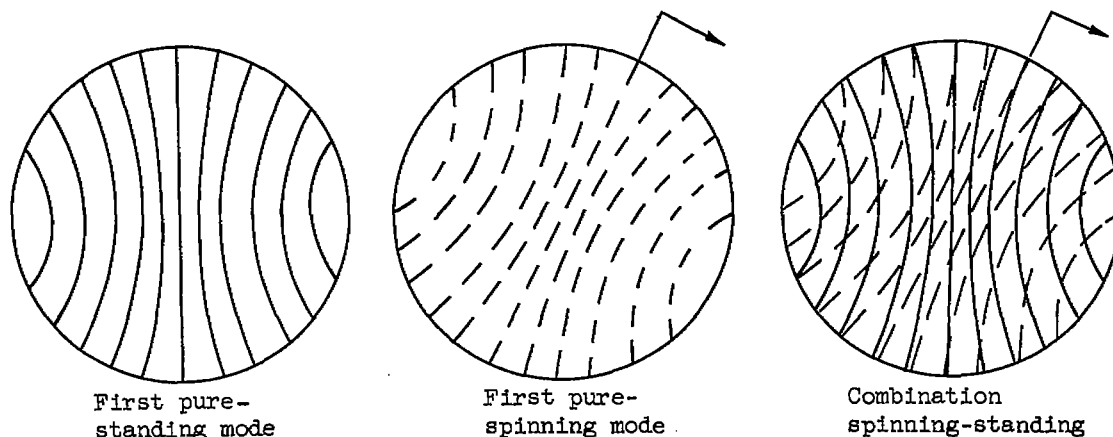
(c)

The equation for pressure fluctuation used in reference 4 shows that the combination spinning-standing mode can be described by two spinning modes of unequal amplitudes rotating in opposite directions. Similarly, the pure-standing mode can be represented by two spinning modes of equal amplitude rotating in opposite directions. Experimental evidence suggests that the first spinning-standing mode usually occurs in symmetrical combustors, while the first standing mode occurs in combustors having a sufficient degree of combustion assymetry. For simplicity, only the first pure-standing tangential mode will be considered.

As shown in appendix B, the pressure fluctuation field in the first pure-standing mode may be described in terms of the root-mean-square pressure fluctuation:

$$\frac{\sqrt{\overline{p^2}}}{\sqrt{\overline{p_R^2}} \cos \theta} = 1.718 \ J_1\left(1.841 \ \frac{r}{R}\right) \tag{1}$$

where $\sqrt{\overline{p^2}}$ is the root-mean-square pressure fluctuation at the cylindrical coordinates (r,θ), $\sqrt{\overline{p_R^2}}$ is the root-mean-square sound pressure at the pressure antinodes, and $J_1(\ )$ is the Bessel function of the first kind and first order. (All symbols are defined in appendix A.) The coordinate system is
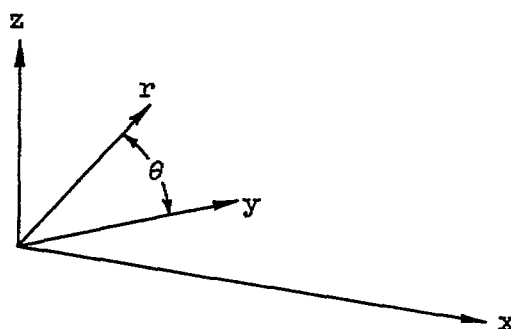
(a)

The pressure parameter $\sqrt{\overline{p^2}}\Big/\sqrt{\overline{p_R^2}}$ $\cos\theta$ given by equation (1) is shown in figure 1 as a function of the fraction of duct radius r/R.

Particle Velocity

Equations are derived in appendix B which relate the transverse particle velocity components v_r and v_θ to the sound-pressure level of the acoustic field. In order to illustrate the relative magnitude of the particle velocity across the duct, equations are derived in appendix B for the root-mean-square particle velocity components $\sqrt{\overline{v_r^2}}$ and $\sqrt{\overline{v_\theta^2}}$:

$$\sqrt{\overline{v_r^2}} = 0.859\,\frac{a}{\gamma}\,\frac{\sqrt{\overline{p_R^2}}}{p_0}\left[J_0\left(1.841\,\frac{r}{R}\right) - J_2\left(1.841\,\frac{r}{R}\right)\right]\cos\theta \qquad (2)$$

$$\sqrt{\overline{v_\theta^2}} = 0.9335\,\frac{a}{\gamma}\,\frac{\sqrt{\overline{p_R^2}}}{p_0}\,\frac{R}{r}\,J_1\left(1.841\,\frac{r}{R}\right)\sin\theta \qquad (3)$$

The root-mean-square particle velocity components expressed by equations (2) and (3) are shown in figure 1.

At the duct axis, the resultant transverse particle velocity is

$$\sqrt{\overline{v_c^2}} = 0.859 \frac{a}{\gamma} \frac{\sqrt{\overline{p_R^2}}}{p_0} \tag{4}$$

This resultant particle velocity is shown in figure 2 for a range of

sound-pressure levels $\sqrt{\overline{p_R^2}}/p_0$ and a range of values of a and γ.

As can be seen from figure 2, the particle velocities at the duct axis are of the same order of magnitude as the stream velocity for the conditions commonly encountered in screeching or screaming combustors.

In summary, the magnitude of the root-mean-square particle velocity at the duct center can be determined from figure 2 for particular sound field and ambient stream conditions. The variation of root-mean-square particle velocity in the duct cross section is illustrated in figure 1 where particle velocity profiles are shown along the duct radius.

Oscillation Frequency

The frequency of acoustic oscillations in the first pure-standing mode is given by the expression (ref. 6, p. 398)

$$f = \frac{0.293a}{R} \tag{5}$$

This frequency is shown in figure 3 for a range of duct radii and for a range of the speed of sound a.

Nonuniformity of Transverse Mode in Realistic Combustors

In realistic combustors the acoustic field may depart from the ideal, uniform transverse mode described in the preceding sections. For example, data reported in reference 2 show a considerable attenuation and phase shift upstream of the flame in a connected-pipe 6-inch screeching combustor. A theoretical analysis described in reference 7 predicts an attenuation upstream of the combustion zone, but no phase shift. The attenuation in both of these cases is due to the change in the speed of sound between the burned and unburned gases and to the lack of a sufficiently strong closed-end condition at the combustor inlet. The

application of the present analysis to realistic combustors must be limited to those cases where the acoustic field sufficiently approximates the pure-standing transverse mode.

TURBULENT MIXING IN A TRANSVERSE ACOUSTIC FIELD

The point-source model is developed in this section to obtain mixing equations which define the fuel-oxidant (or fuel-air) ratio at points downstream as a function of time, gas stream velocity, and turbulence parameters. The transverse displacement of the concentration wake by the particle velocity is defined for vapor injection at any point in the inlet station of the simulated cylinder combustor. Finally, the transverse displacement of the concentration wake is included in the mixing equation so that the fuel-oxidant ratio is defined as a function of the stream and acoustic field parameters.

Turbulent Mixing From a Point Source

The concentration C at any point (X,Y,Z) downstream from a point source emitting vapor at the rate w_f into a gas stream of homogeneous turbulence is (ref. 8)

$$C = \frac{w_f}{(4\pi)^{3/2}} \int_0^\infty \frac{1}{\omega^{3/2}} e^{-\frac{(X-Ut)^2+Y^2+Z^2}{4\omega}} dt \qquad (6)$$

It is assumed that the vapor attains the stream velocity immediately after injection. In terms of fuel-oxidant or fuel-air ratio f/A equation (6) becomes

$$\frac{\rho_0(f/A)}{w_f} = \frac{1}{(4\pi)^{3/2}} \int_0^\infty \frac{1}{\omega^{3/2}} e^{-\frac{(X-Ut)^2+Y^2+Z^2}{4\omega}} dt \qquad (7)$$

where U is the stream velocity, t the residence time, and ω the turbulent spreading coefficient.

As discussed in reference 8, the turbulent spreading coefficient is a function of the residence time t, the turbulence intensity $\sqrt{\overline{v_T^2}}$, and the Lagrangian correlation coefficient $\mathcal{R}$. In the present analysis, the Lagrangian correlation coefficient will be assumed to have the form

$$\mathcal{R} = e^{-t/t^*}$$

where $t^* = \mathscr{L}/\sqrt{v_T^2}$ and $\mathscr{L}$ is the Lagrangian scale of turbulence. With this assumption and with the equations for ω given in reference 8, the spreading coefficient becomes

$$\omega = \mathscr{L}^2 \left[\frac{\sqrt{v_T^2}}{\mathscr{L}} t - 1 + e^{-\frac{\sqrt{v_T^2}}{\mathscr{L}} t} \right] \tag{8}$$

The spreading coefficient given by equation (8) is shown in figure 4 as a function of the turbulence intensity and scale. For convenience in physical interpretation, ω is plotted against distance downstream $x = Ut$, but must be treated as a function of time in equations (6) and (7). The figure shows that near the injector the spreading coefficient depends only on the turbulence intensity $\sqrt{v_T^2}/U$ and residence time. For the lower intensities, the spreading coefficient is relatively independent of turbulence scale even at distances far downstream, so that in approximation the turbulence scale need be estimated only roughly.

Injection on Duct Axis

The analysis in reference 5 provides equations describing the motion of a mixing wake imposed by a plane transverse sound wave. The analysis assumes that the root-mean-square particle velocity $\sqrt{v^2}$ is constant in the region encompassing the deformed wake. The particle velocity profiles in figure 1 show that, if the point source is located on the duct axis and if the wake is not displaced too far from the duct axis, the condition is approximately met so that the displacement y of the concentration wake is given by

$$y = y_{max} \sin\left(\frac{\pi f X}{U}\right) \sin\left(2\pi f \tau - \frac{\pi f X}{U}\right) \tag{9}$$

where

$$y_{max} = \frac{\sqrt{2}\ \sqrt{v^2}}{\pi f} \tag{10}$$

The ratio y/y_{max} is shown in figure 5(a) as a function of the dimensionless axial distance $f X/U$ and the fractional cycle $f\tau$. The transverse motion of the concentration wake is cyclic and produces definite nodes at whole number multiples of the dimensionless distance $f X/U$.

The maximum wake displacement y_{max}, which occurs at the antinodal stations, is plotted in figure 5(b) for a range of particle velocities and oscillation frequencies.

An expression relating y_{max} to the duct radius R and the sound pressure $\sqrt{p_R^2}$ in the first pure-standing tangential mode may be obtained by combining equations (4) and (5) with equation (10):

$$\frac{y_{max}}{R} = \frac{1.32}{\gamma} \frac{\sqrt{p_R^2}}{p_0} \qquad (11)$$

Comparison of equation (11) with figure 1 shows that, for moderately high acoustic amplitudes (say, $\sqrt{p_R^2}/p_0 \approx 0.2$), the assumption of constant particle velocity is fairly good.

The magnitude of the pressure fluctuations encountered by the mixing wake during its transverse motion about the duct axis will be of interest in later discussion. The magnitude of the pressure fluctuation $\sqrt{p^2}$ at the extreme wake displacement y_{max} can be estimated by evaluating equation (1) at $r = y_{max}$ along the line $\theta = 0$, and substituting y_{max} from equation (11):

$$\frac{\sqrt{p^2}}{p_0} = 1.718 \frac{\sqrt{p_R^2}}{p_0} J_1\left(\frac{2.43}{\gamma} \frac{\sqrt{p_R^2}}{p_0}\right) \qquad (12)$$

The pressure fluctuation at y_{max} expressed by equation (12) is shown in figure 6 as a function of the pressure ratio $\sqrt{p_R^2}/p_0$ and of γ. From figure 6, it is seen that, for injection on the duct axis, the mixing wake encounters only small pressure fluctuations when the sound field has a moderate amplitude.

From the preceding discussion and from the derivation in reference 5, a mixing equation may be written for injection at the duct axis. This expression is an extension of equation (7) and accounts for the deformation of the mixing wake by inclusion of the transverse displacement of the wake center y:

$$\frac{p_0(f/A)}{w_f} = \frac{1}{(4\pi)^{3/2}} \int_0^\infty \frac{1}{\omega^{3/2}} e^{-\frac{(X-Ut)^2+(Y-y)^2+Z^2}{4\omega}} dt \qquad (13)$$

where ω is given by equation (8) and y by equations (9) and (10).

Injection at Points Away from Duct Axis

If the point source of injection is placed at a point away from the duct axis, the "solid-body" motion expressed by equation (9) no longer obtains. The pressure gradient encountered by the wake exerts an alternately compressive and expansive motion in the transverse direction so that the gaussian fuel-oxidant profile expressed by equation (9) will be altered. This effect can be described by deriving the exact expression for particle motion along the line $\theta = 0$. The particle velocity along $\theta = 0$ is given by equation (B19) which may be rewritten:

$$\frac{dy}{d\tau} = 1.215 \frac{a}{\gamma} \frac{\sqrt{p_R^2}}{p_0} \left[J_0\left(1.841 \frac{y}{R}\right) - J_2\left(1.841 \frac{y}{R}\right) \right] \sin(2\pi f\tau) \qquad (14)$$

By separating the variables and integrating over the distance $y_2 - y_1$ travelled by a particle during the time interval $\tau_2 - \tau_1$, there results:

$$\int_{y_1/R}^{y_2/R} \frac{d(y/R)}{J_0\left(1.841 \frac{y}{R}\right) - J_2\left(1.841 \frac{y}{R}\right)} = \frac{0.66}{\gamma} \frac{\sqrt{p_R^2}}{p_0} \int_{\tau_1}^{\tau_2} \sin(2\pi f\tau) d\tau \qquad (15)$$

If $f\tau_1 = 0$ and $f\tau_2 = 1/2$, equation (13) represents the maximum displacement of any particular particle in the direction towards the wall:

$$\int_{y_1/R}^{y_2/R} \frac{d(y/R)}{J_0\left(1.841 \frac{y}{R}\right) - J_2\left(1.841 \frac{y}{R}\right)} = \frac{1.32}{\gamma} \frac{\sqrt{p_R^2}}{p_0} \qquad (16)$$

Equation (16) expresses the maximum displacement of a particle starting from any point y_1 at time $\tau = 0$. The integral in equation (16) was evaluated numerically to obtain a curve such as shown in the following sketch:

(e)

A fluid particle initially at y_1 moves to y_2 during the same time interval in which a particle initially at y_3 moves to y_4. From the sketch it can be seen that, in a given time interval, a particle initially at y_1 at one side of the wake moves farther than another particle initially at y_3 on the other side of the wake. To estimate the degree of departure from the solid-body motion, the ratio $(y_4 - y_3)/(y_2 - y_1)$ is shown in figure 7 as a function of the initial position of the wake center $(y_1 + y_3)/2$, the sound pressure $\sqrt{p_R^2}$, and the initial separation of the particles $y_3 - y_1$. The sound pressure $\sqrt{p_R^2}$ has little effect in the range shown, while the initial separation has a large effect. For small initial particle separation, the solid-body motion is closely approximated for point-source positions as much as halfway to the wall.

The compressive effect of pressure gradient on the fuel-oxidant profile across the mixing wake was investigated further by means of a simple model. It was assumed that the mixing from a point source had produced a given concentration profile centered on the injector axis. Then the acoustic field was assumed to act on the wake, pushing it alternately toward the duct axis and the duct wall. At the initial position, the profile was assumed to have a gaussian form such as given by the approximate solution of equation (7) given in reference (8):

$$\frac{\rho_0(f/A)}{w_f} = \frac{1}{4\pi U \omega_X} e^{-\frac{X^2+(y-y_i)^2}{4\omega_X}} \tag{17}$$

where y_i is the lateral distance from the duct axis to the point of injection, ω_X was evaluated at $X = 1.25$ feet, and U was assumed to

be 500 feet per second. For a given value of the sound-pressure param-
eter 1.32 $\sqrt{\overline{p_R^2}}/\gamma p_0$, the profiles nearest the duct axis and nearest the
duct wall were constructed with the aid of equation (16) and sketch (e).
In using this graphical method, it was noted that, although the density
of a fluid particle changes as it passes along the pressure gradient,
its fuel-oxidant ratio remains constant. The results of this procedure
are shown in figure 8 for two different sets of the injector positions
y_i/R and the sound-pressure parameter 1.32 $\sqrt{\overline{p_R^2}}/\gamma p_0$. The solid lines
in both cases represent the initial gaussian profile directly downstream
of the point of injection. All the dashed lines represent the distorted
profiles when the wake is farthest from the injection axis in both direc-
tions. The distorted profiles have been transposed to the injection axis
to facilitate direct comparison. For the sound pressure and injector
position chosen for figure 8(a), the effect of pressure gradient on the
fuel-oxidant profile was small. When the sound pressure was increased
and the injector position moved farther from the duct axis, a substantial
change occurred in the fuel-oxidant profile as shown in figure 8(b).

In summary, when injection is at the duct axis and when the sound-
pressure level is not too high, the transverse motion of the mixing wake
in the first pure-standing mode is nearly a solid-body motion as described
by equations (9) and (10). When injection is at points considerably away
from the duct axis and when the sound-pressure level is high, the solid-
body motion no longer describes the motion of the mixing wake with accu-
racy. In this case, an accurate description of the motion of the mixing
wake can be obtained by graphical means, but the shape of the fuel-
oxidant profile can only be approximated. When injection is at points
considerably away from the duct axis, a rough approximation of wake mo-
tion can be obtained by using the solid-body motion (eq. (9)) and by
evaluating the particle velocity for that equation at the injector axis
from equation (4).

With vapor injection at points away from the duct axis, pressure
fluctuations at the injector will cause cyclic changes in the fuel-oxidant
ratio. The mixing equation may be corrected for this effect by noting
that the fuel-oxidant ratio of a fluid particle leaving the injector is
proportional to $\rho_0/(\rho_0 + \rho_i)$ where ρ_0 is the ambient mean density and
ρ_i is the density fluctuation at the injector. This density ratio may
be inserted into the mixing equation as follows:

$$\frac{\rho_0(f/A)}{w_f} = \frac{1}{(4\pi)^{3/2}} \int_0^\infty \frac{1}{1 + \dfrac{p_i}{\gamma p_0}} \frac{1}{\omega^{3/2}} e^{-\dfrac{(X-Ut)^2+(Y-y)^2+Z^2}{4\omega}} \, dt \quad (18)$$
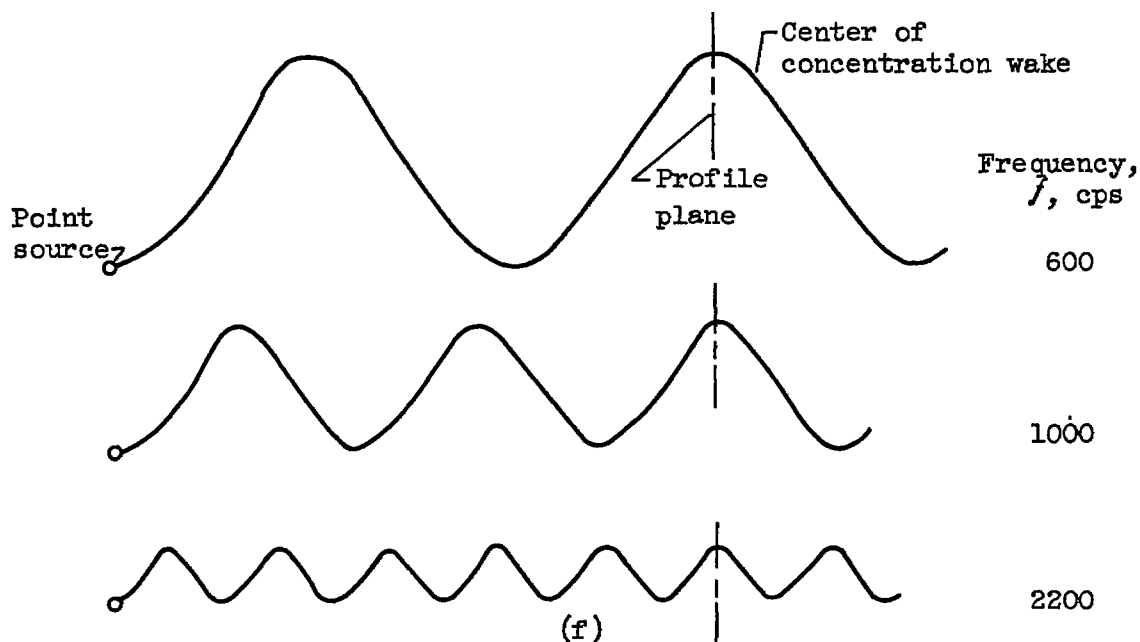
where p_i is the pressure fluctuation at the injector as given by equation (B5). The effect of pressure gradient may be included in equation (18) by using equation (15) to determine y. Equation (18) is not actually used in calculating fuel-oxidant ratios in this report; it is included only to illustrate the effect of pressure fluctuations at the injector.

MIXING IN FIRST PURE-STANDING TANGENTIAL MODE

In this section the mixing equations developed in the preceding section for vapor injection at a point source are applied to acoustic fields and gas streams with properties in the range encountered in screaming or screeching combustors. The effects of sound-pressure level, oscillation frequency, stream velocity, and turbulence on fuel-oxidant patterns are treated for injection at the duct axis in the first pure-standing tangential mode. Injection away from the duct axis is discussed qualitatively. The first pure-standing tangential mode is assumed to exist throughout the length of the simulated combustor, and the gas stream properties are assumed constant throughout the combustor for any particular set of conditions.

Effect of Amplitude and Frequency of Acoustic Oscillations

To investigate the effect of sound-pressure level and frequency, fuel-oxidant ratio profiles were calculated from equation (13) by numerical integration with a high-speed digital computer using Simpson's rule. The profiles were calculated for a fixed axial station $X = 1.25$ feet and for two instants in time $f\tau = 0.5$ and $f\tau = 0.75$. The turbulent

stream properties were fixed at $U = 500$ feet per second, $\sqrt{\overline{v_T^2}}/U = 0.05$,

and $\mathscr{L} = 0.1$ foot, so that $\omega_X = 1.603 \times 10^{-3}$ square foot. The profiles were calculated for a range of particle velocities and oscillation frequencies. The frequencies were chosen so that the axial station $X = 1.25$ feet was an antinodal station in each case. (Antinodal stations are illustrated in fig. 5(a) and are at $fX/U = 0.5, 1.5, \ldots$) Antinodal stations were chosen for the calculations because the wake attains its maximum lateral displacement there. The group of fuel-oxidant ratio profiles calculated for $f\tau = 0.5$ are shown in figure 9(a) and have the following geometrical relation to the mixing wake:

Point source

Profile plane

Center of concentration wake

Frequency, f, cps

600

1000

2200

(f)

As shown by sketch (f), increases in frequency reduce the lateral displacement and internodal distances of the wake.

In figure 9(b), the wake motion has progressed one-quarter cycle to $f\tau = 0.75$, and the calculated fuel-oxidant profile lies in a plane normal to the wake center:

Point source

Profile plane

Center of concentration wake

Frequency, f, cps

600

1000

2200

(g)
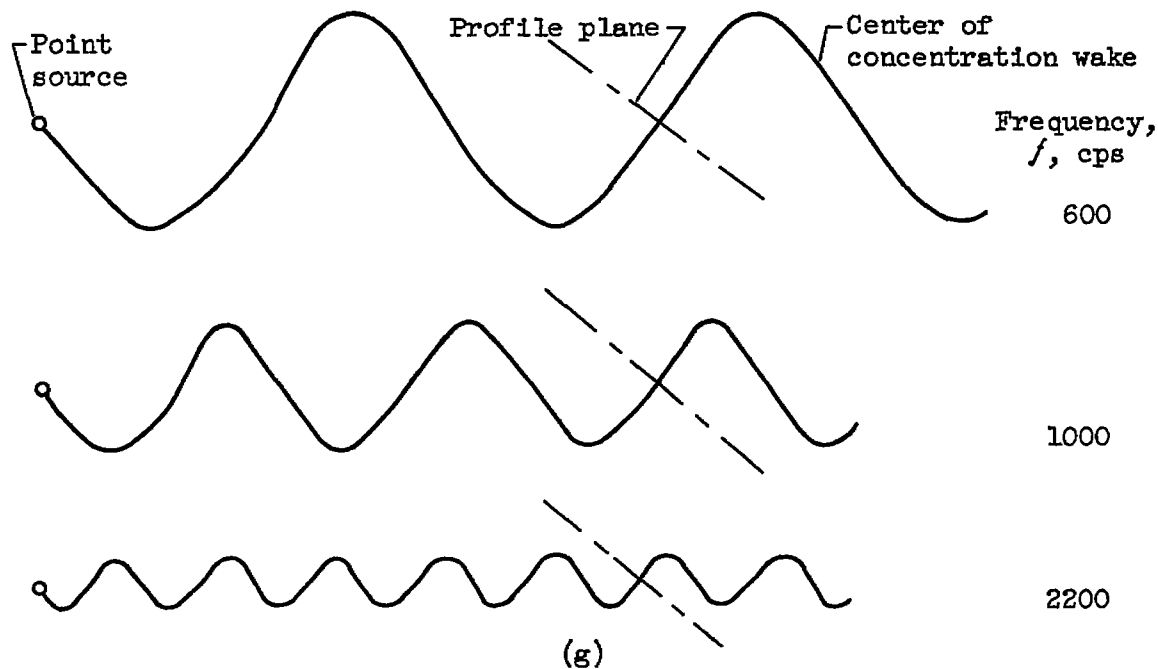
The profiles were calculated for planes normal to the wake center to facilitate comparison with the profiles in the absence of screech (solid lines in fig. 9(b)). For a frequency of 2200 cycles per second, the rise in fuel-oxidant ratio to the left of center in the curve for $\sqrt{\overline{v^2}} = 600$ feet per second is due to the preceding wake wrinkle.

As the particle velocity is increased, the peak fuel-oxidant ratio decreases in all cases shown in figure 9. In addition to this general decrease in fuel-oxidant ratio, a cyclic change in fuel-oxidant ratio is also shown. (The profiles in fig. 9(a) will be repeated at $f\tau = 0$ and those in fig. 9(b) will be repeated at $f\tau = 0.25$.) As shown in reference 5, the fuel-oxidant ratio will be highest in portions of the wake having zero slope and lowest in portions having maximum slope. This indicates that the fuel-oxidant ratios shown for $f\tau = 0.5$ (fig. 9(a)) will form the upper limit of the cyclic variation, and the fuel-oxidant ratios in figure 9(b) will form the lower limit. By comparison of figures 9(a) and (b) it can be seen that the magnitude of the cyclic variation in fuel-oxidant ratio is greatest for the lower oscillation frequency and increases with particle velocity.
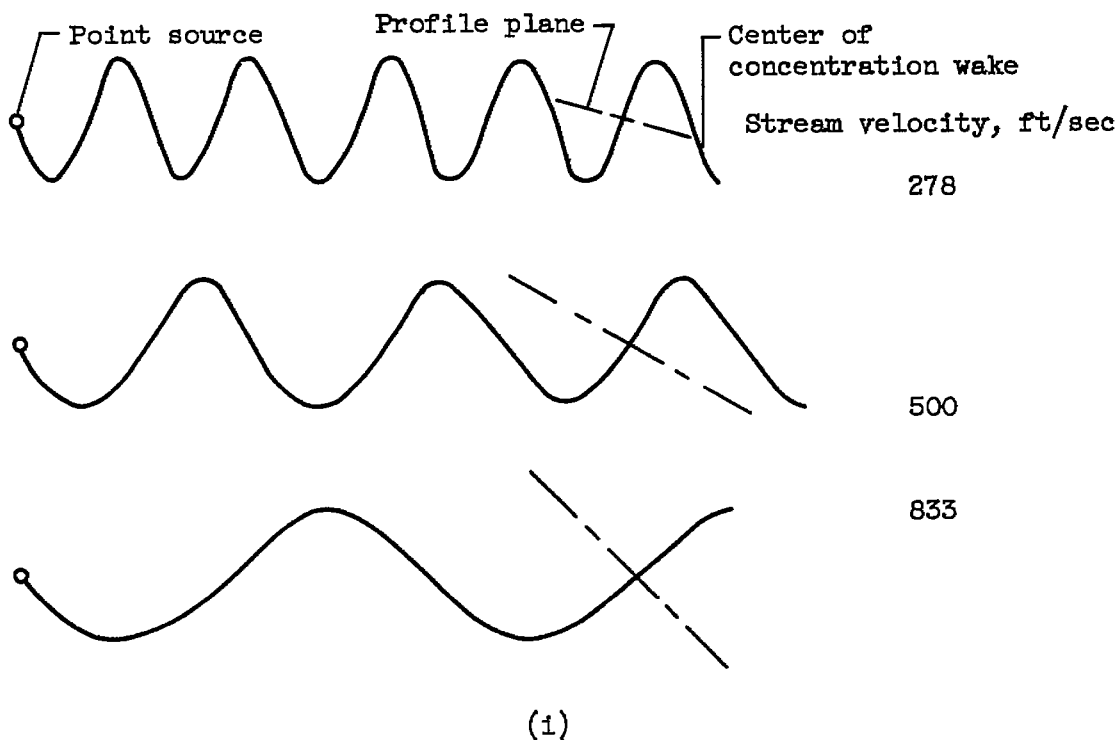
Consideration of figures 5 and 9 shows that a time and position relation exists between the fuel-oxidant and pressure fluctuation. When the wake is at its maximum lateral displacement, the fuel-oxidant ratio at the antinodal stations is at a maximum, and the pressure is also at a maximum. This relation is expressed by equation (B26), derived in appendix B, which defines the pressure change experienced by the wake center during its transverse motion. The pressure fluctuation calculated from equation (B26) is shown in figure 10 in comparison to fuel-oxidant fluctuations obtained from figure 9. This comparison is made for two axial stations: $fX/U = 0.5, 1.5, \ldots$ and $fX/U = 0.75, 1.75, \ldots$. At the antinodal stations $fX/U = 0.5, 1.5, \ldots$, the pressure and fuel-oxidant fluctuations are exactly in phase as shown in figure 10(a). At stations away from the antinodal, such as $fX/U = 0.75, 1.75, \ldots$ (fig. 10(b)), the pressure and fuel-oxidant fluctuations are no longer in phase, but the magnitude of the pressure fluctuation is considerably reduced.

Effect of Stream Velocity

The effect of stream velocity on the mixing pattern is shown in figure 11 in which fuel-oxidant profiles are shown for the axial station X = 1.25 feet for two instants in time $f\tau = 0.5$ and $f\tau = 0.75$. The profiles were calculated for a fixed oscillation frequency of 1000 cycles per second and a spreading coefficient of 1.603×10^{-3} square foot. The geometry of the concentration wake and fuel-oxidant profile for figure 11(a) is:

Profile | ┌ Center of
plane ┐| | concentration wake

┌ Point source

Stream velocity,
ft/sec

278

500

833

(h)
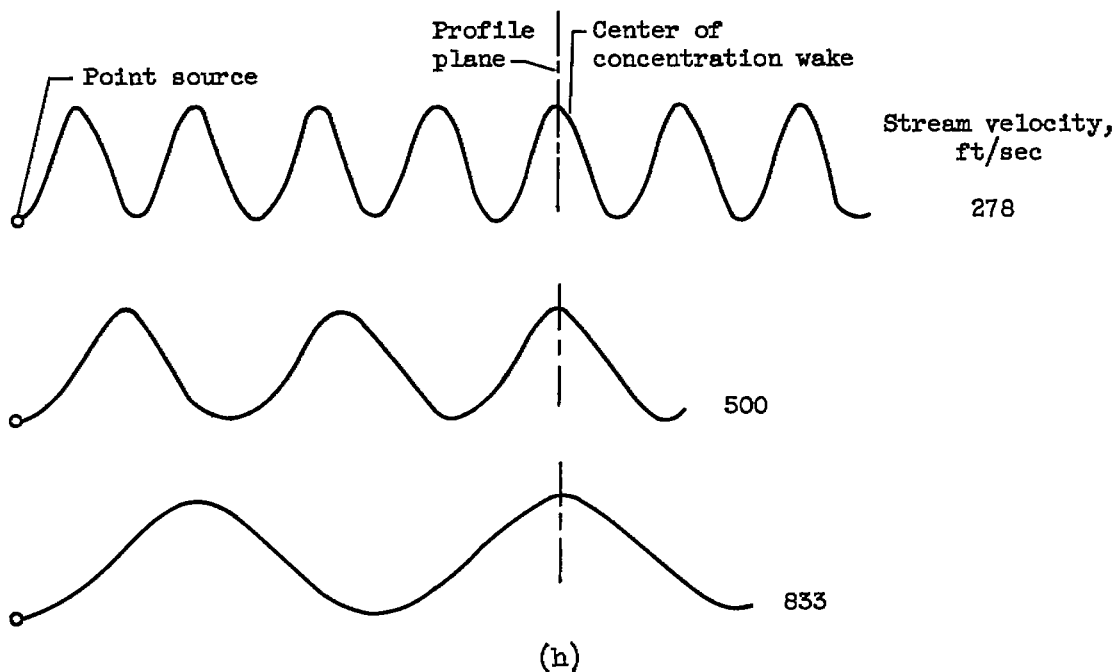
In figure 11(b) the wake motion has progressed one-quarter cycle, and
the calculated fuel-oxidant profile lies in a plane normal to the wake
center:

┌ Point source   Profile plane ┐   ┌ Center of
                                              concentration wake

Stream velocity, ft/sec

278

500

833

(i)

Comparison of figures 11(a) and (b) shows that stream velocity has an effect on fuel-oxidant ratio similar to that of oscillation frequency as discussed in the preceding section. The general decrease in fuel-oxidant ratio with stream velocity is more marked than that with oscillation frequency. A cyclic fluctuation in fuel-oxidant ratio is again noted and is most pronounced for the lower stream velocity.

Effect of Turbulence and Residence Time

The effect of turbulence parameters is illustrated in figure 12 where fuel-oxidant profiles are shown for two sets of turbulence conditions. The profiles were calculated for a stream velocity of 500 feet per second, an oscillation frequency of 1000 cycles per second, a time of $\sqrt{\tau} = 0$, and an axial station $X = 1.25$ feet. The peak fuel-oxidant ratio has the same percentage decrease as the particle velocity increases in both cases. From this observation, it is concluded that for the range of conditions investigated the turbulence does not affect the mixing in any way other than normal turbulent mixing.

Since the spreading coefficient is also a function of residence time, it also may be concluded that, for the range of conditions investigated, the residence time, or distance downstream, does not affect the mixing in any but the usual manner.

Injection at Points Away from Duct Axis

As discussed in the earlier section titled Injection at Points Away from Duct Axis, injection at points away from the pressure node introduces a pressure fluctuation effect as expressed by equation (18). A qualitative picture of this effect is illustrated in figure 13 where the fuel-oxidant wake is shown for successive intervals of time along with the pressure fluctuation curve. The width of the wake represents the magnitude of the peak fuel-oxidant ratio. When the pressure fluctuation is negative, the fuel-oxidant ratio at the injector is high, but is low when the pressure fluctuation is positive. The figure shows that, when the richest portion of the wake has reached its maximum excursion towards the duct wall, the pressure fluctuation has reached its maximum positive value. A second, lesser maximum of fuel-oxidant ratio reaches its maximum excursion towards the duct center when the pressure is at its other maximum positive value. In this way, the pressure fluctuations at the injector accentuate the fuel-oxidant ratio fluctuations previously discussed in the section Effect of Amplitude and Frequency of Acoustic Oscillations.

POSSIBLE MECHANISMS CONTRIBUTING TO SCREECH AND SCREAM

The complexity of the aerodynamic and chemical processes which occur in a combustor has prevented the formulation of a straightforward, all

inclusive description of the screech and scream driving mechanisms. The role of pressure fluctuations in driving screech is discussed in reference 2 where it is suggested that a periodic change in pressure is expected to cause an even larger periodic change in heat-release rate. Consideration of the equation for chemical-reaction rate indicates that fuel-oxidant fluctuations would also cause fluctuations in heat-release rate. For example, consider the second-order reaction rate:

$$\text{Reaction rate} \sim C_A^2 (f/A) e^{-E/R_c T} \tag{19}$$

where C_A is the initial concentration of oxidant, E the activation energy, R_c the gas constant, and T the flame temperature. The flame temperature is a strong function of the fuel-oxidant ratio so that the heat-release curve has the following form:
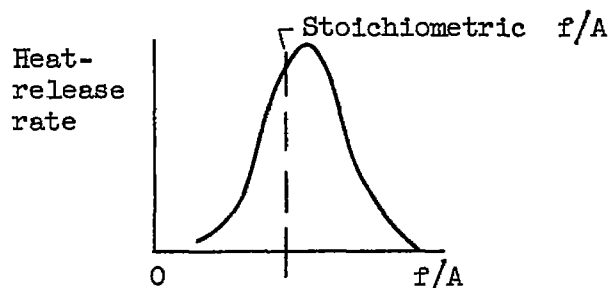
(j)

The pressure and fuel-oxidant ratio driving mechanisms are only two of a number of possible screech and scream driving mechanisms. Other mechanisms are described in references 9 and 10.

The results of the present analysis have shown that the fuel-oxidant mixing wake downstream of the injectors is affected by transverse acoustic oscillations in two principal ways:

(1) The fuel-oxidant mixing wake is given an oscillatory transverse motion which is quite large for moderate screech or scream intensities.

(2) During its transverse motion at antinodal stations, the mixing wake undergoes periodic changes in fuel-oxidant ratio which are exactly in phase with the pressure fluctuations.

With fuel injection at the duct axis, the fuel-oxidant fluctuations caused by the transverse acoustic oscillations may be more important to the screech or scream driving mechanism than the fluctuations in pressure.

As shown in figure 6, the pressure fluctuations encountered by the mixing wake during its transverse motion are quite small with injection at the duct axis, but as shown in figure 10, the fuel-oxidant fluctuations may be quite large for this case. These observations and results suggest that the actions of the mixing wake may be important to the driving mechanism of screech and scream. To pursue this notion further, possible screech and scream mechanisms are discussed in detail in this section, and methods for their control are suggested.

In the case of ramjet combustors and afterburners where injectors are positioned upstream of flameholders, the axial distance between the injector and flameholder stations may be of critical importance to the screech mechanism. As shown in figure 5 the mixing wake may be periodically displaced a considerable lateral distance at antinodal axial distances from the point of injection. If the distance from the injector to the flame front is at or near a wake antinodal distance, then the fuel-air mixture might pass alternately back and forth across the flameholder and cause significant periodic changes in heat release in the two opposing flame fronts. The prevention or control of this type of screech mechanism may lie in the distance from the injector to the flame front. By changing this distance by a fraction of the internodal distance, the time and position phase relation between the fuel-oxidant ratio fluctuations and pressure fluctuations might be altered to attain a suppressing effect on the screech driving mechanism.

The possibility of contributions to screech by periodic fuel-air ratio fluctuations is discussed in this paragraph. Unpublished NACA data on full-scale combustor operation, shown in figure 14, show that screech occurred at lean over-all fuel-air ratios. In the absence of screech, the peaks in the fuel-air ratio profile at the flame front may be expected to be at stoichiometric or lower for such lean over-all fuel-air ratios:
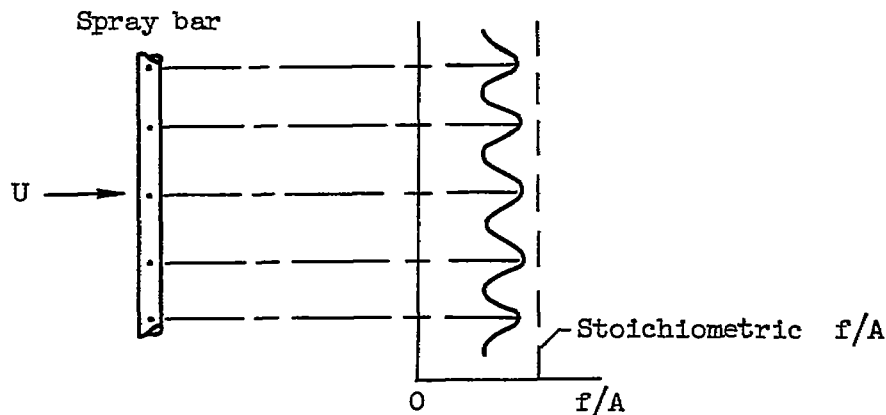
(k)

In the section MIXING IN FIRST PURE-STANDING TANGENTIAL MODE, it was shown
that transverse acoustic oscillations cause both a general decrease in
peak fuel-air ratio at any station downstream from the injection station
and a periodic fluctuation in peak fuel-air ratio at antinodal stations,
which is in phase with the pressure fluctuations. This situation is
illustrated in sketch (l):

Spray bar

U →

─Stoichiometric f/A

0   f/A

Heat-
release
rate

─Stoichiometric f/A

0   f/A

(l)
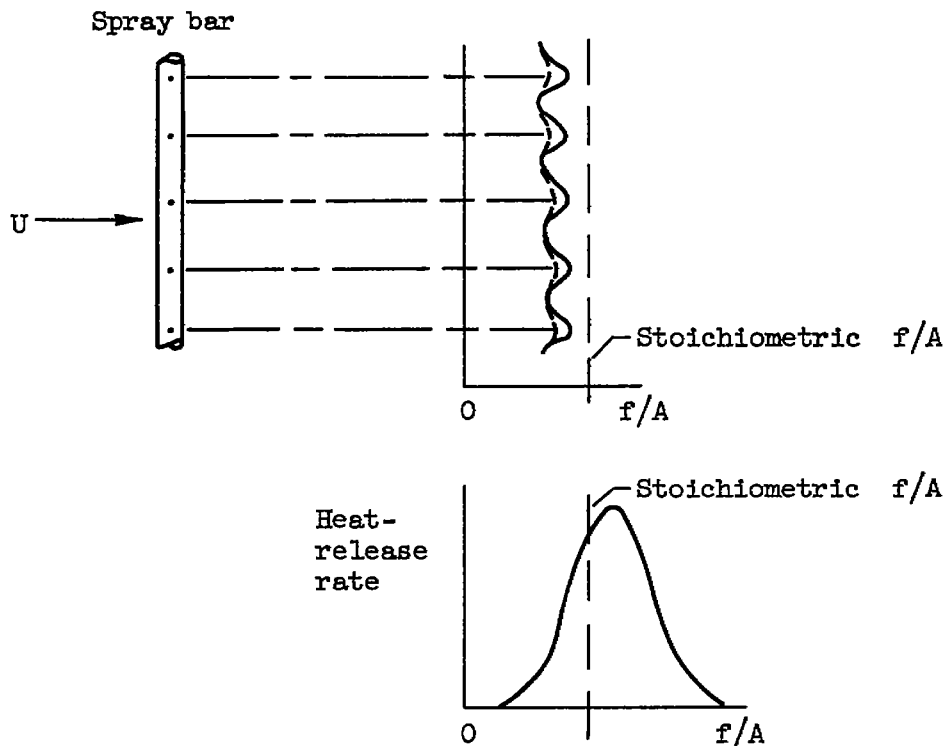
The fuel-air ratio profile shown by the solid line represents the upper
limit of the fuel-air ratio fluctuation, and the dotted line represents
the lower limit. The fuel-air ratio profile shown is assumed to be at
the flame front, which is at one of the antinodal distances $fx/U = 0.5$,
1.5, . . . downstream from the spray bar. Since the mean fuel-air ratio
profile is lower than stoichiometric, a fluctuation towards higher fuel-
air ratio will result in an increased heat-release rate as shown by the
reaction rate curve above. This increase in heat release due to a rise
in fuel-air ratio is directly in phase with the increase in heat release
due to pressure rise, so that the screech is driven to even higher
amplitude. If the mean fuel-air ratio were higher than stoichiometric,
then a rise in fuel-air ratio would tend to decrease the heat-release

rate and thus exert a suppressing effect on the screech driving mechanism. To obtain a mean fuel-air ratio higher than stoichiometric, the number of injection points could be reduced with a higher fuel flow rate through each:

Spray bar

U →

Stoichiometric

O   f/A
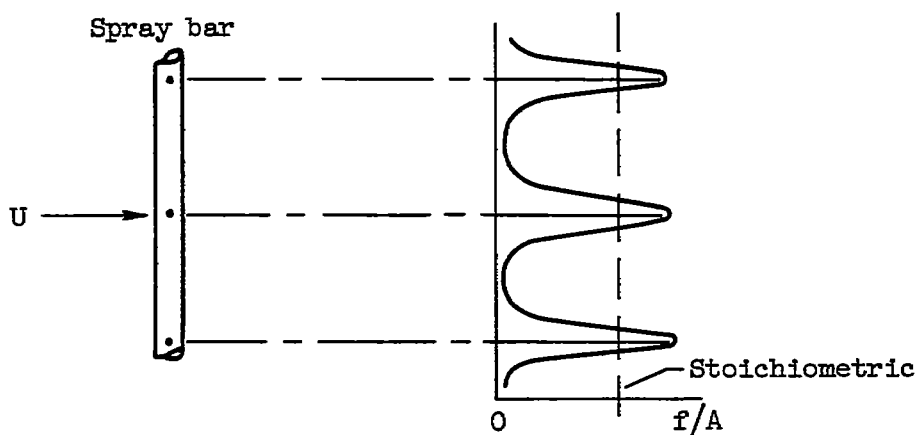
(m)

An alternate method could be to move the original spray bar downstream:

Spray bar

U →

Stoichiometric

O   f/A
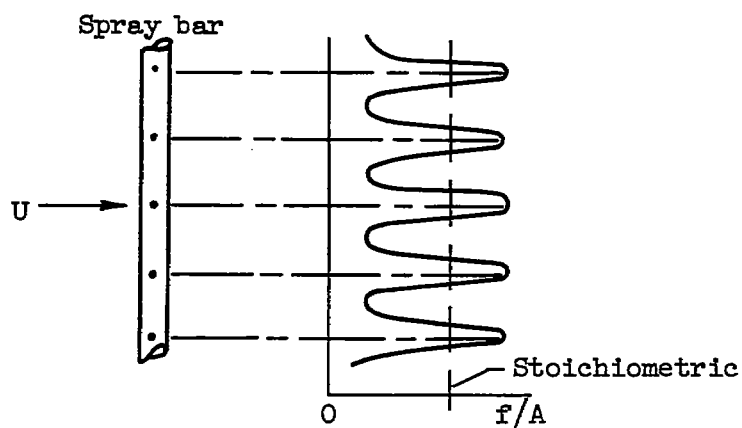
(n)

Another method of suppressing the effect of fuel-air ratio fluctuations is control of the fuel-flow rate. The stretching of the mixing wake by the acoustic oscillations could be compensated by mechanically varying the fuel flow rate in proper time-phase relation with the pressure fluctuations. Overcompensation of the stretching effect would cause a phase inversion of the fuel-air ratio and pressure relation, thus tending to suppress further the screech driving mechanism.

The effect of offcenter injection on fuel-oxidant ratio fluctuations has been discussed in the second section titled Injection at Points Away from Duct Axis, where it was shown that the pressure fluctuation at the injector produces fuel-oxidant ratio fluctuations in phase with those caused by the deformation of the mixing wake by particle velocity. It should be noted here that the transverse particle velocity decreases as the injection axis is moved away from the duct axis in the first pure-standing tangential mode. Since the particle velocity decreases, the magnitude of the fuel-oxidant ratio fluctuations will also decrease as shown previously. From these considerations it appears that, as the fuel injector is moved away from the pressure node, the changes in magnitude of the pressure fluctuation and particle velocity act in a manner to compensate each other, thus diminishing the effect of change in injector position on the fuel-oxidant ratio fluctuations. If this compensation is exact, then the fuel-oxidant ratio fluctuations will be of the same magnitude as obtained with injection at the pressure node. However, the mixing wake will encounter more severe pressure fluctuations during its transverse motion so that the screech driving mechanism might be strengthened by positioning the injector away from the duct axis.

CONCLUSIONS

In summary, equations have been derived for the calculation of fuel-oxidant ratio profiles downstream from injectors simulating point sources in combustors with transverse acoustic oscillations.

For combustors having the first pure-standing tangential mode of acoustic oscillation and injection occurring on the combustor axis, the following conclusions are made:

1. Acoustic oscillations of the magnitude present in screeching or screaming combustors can cause considerable transverse motion and distortion of the fuel-oxidant mixing wake.

2. In general, the peak fuel-oxidant ratio is lowered by the transverse acoustic oscillations. For example, when the peak-to-peak amplitude of the pressure fluctuation is equal to the mean chamber pressure, the peak fuel-oxidant ratio may be reduced as much as 60 percent in a gas stream at 4000° R flowing at 300 feet per second in a 2-foot-diameter duct.

3. The decrease in peak fuel-oxidant ratio becomes more marked as the amplitude of the acoustic oscillation increases.

4. The decrease in peak fuel-oxidant ratio becomes more marked as the stream velocity decreases.

5. At any particular combustor station, the peak fuel-oxidant ratio has a cyclic variation with time. The phase relation between the peak fuel-oxidant ratio and pressure fluctuations is a function of the position of the station, the stream velocity, and the oscillation frequency. For the cases of low oscillation frequency and low stream velocity or both, the portions of the mixing wake which are displaced farthest from the duct axis have a cyclic variation in fuel-oxidant ratio which is exactly in phase with the pressure fluctuations (i.e., maximums of fuel-oxidant ratio and acoustic pressure occur at the same time).

For combustors where injection occurs at other than the pressure node of the first pure tangential mode of acoustic oscillation, the following conclusion is made:

1. With constant fuel injection rate, the pressure fluctuations at the point of injection accentuate the fuel-oxidant fluctuations at stations downstream.

Lewis Flight Propulsion Laboratory
    National Advisory Committee for Aeronautics
        Cleveland, Ohio, March 18, 1957

APPENDIX A

SYMBOLS

A   constant

a   speed of sound, ft/sec

C   concentration of diffusing vapor, lb/cu ft

C_A initial concentration of oxidant

E   activation energy

e   Naperian base

f frequency, or frequency of combined transverse and axial nodes, cps

$f_{m,n}$ frequency of combined transverse modes, cps

f_x frequency of axial mode, cps

f/A   fuel-air or fuel-oxidant ratio by weight

$J_n(\ )$ Bessel function, first kind, order n

L   length of cylindrical duct, ft

$\mathscr{L}$ Lagrangian scale of turbulence, ft

m   wave number for radial mode

n   wave number for tangential mode

n_x wave number for axial mode

p   sound-pressure fluctuation, lb/sq in.

p_i pressure fluctuation at injector, lb/sq in.

p_0 ambient mean static pressure, lb/sq in.

$\sqrt{\overline{p^2}}$ root mean square of sound-pressure fluctuation, lb/sq in.

$\sqrt{\overline{p_R^2}}$ root mean square of sound-pressure fluctuation at pressure anti-node, lb/sq in.

R   radius of cylindrical duct, ft

R_c gas constant

$\mathscr{R}$ Lagrangian turbulence correlation coefficient

r   radial coordinate in cylindrical coordinate system, ft

T   flame temperature

t   residence time in fluid stream, sec

t*   characteristic time of turbulence, sec

U   stream velocity, ft/sec

v   resultant particle velocity, ft/sec

v_c resultant particle velocity along duct axis, ft/sec

v_r radial particle velocity, ft/sec

v_θ tangential particle velocity, ft/sec

$\sqrt{\overline{v^2}}$ root mean square of particle velocity, ft/sec

$\sqrt{\overline{v_T^2}}$ intensity of turbulence, ft/sec

w_f fuel flow rate from point source, lb/sec

X,Y,Z   position of particular point in rectangular coordinates, ft

x   axial coordinate in cylindrical coordinate system, ft

y   lateral displacement of mixing wake center, ft

y_i lateral distance from duct axis to point of injection, ft

y_{max} maximum lateral displacement of mixing wake center, ft

$\alpha_{m,n}$ roots of the equation $[dJ_m(\pi\alpha)/d\alpha] = 0$

γ ratio of specific heats

θ angle of cylindrical coordinates, radians

ρ_i density fluctuation at point source, lb/cu ft

ρ_0 mean ambient density, lb/cu ft

τ time scale of acoustic oscillations, sec

ω turbulent spreading coefficient, sq ft

ω_X turbulent spreading coefficient at axial station X, sq ft

APPENDIX B

DERIVATION OF EQUATIONS

Pressure Fluctuation

The general solution of the wave equation for the pressure fluctuation p is given in reference 6 (p. 398):

$$p = - \sum_{m,n,n_x} p_0 A J_n \left(\frac{2\pi f_{m,n}}{a} r \right) \cos (n\theta) \cos \left(\frac{2\pi f_x x}{a} \right) e^{-i2\pi f \tau} \tag{B1}$$

where the minus sign is used for convenience in later analysis and where the cylindrical coordinate system (x, r, θ) is used. The various frequencies are

$$f_{m,n} = \frac{\alpha_{m,n} a}{2R}, \quad f_x = \frac{n_x a}{2L}, \quad f = \sqrt{f_{m,n}^2 + f_x^2} \tag{B2}$$

where the values of $\alpha_{m,n}$ are given in reference 6 (p. 399). The m, n, and n_x are wave numbers for the radial, tangential, and axial modes, respectively.

The expression for the pressure fluctuation in the first pure-standing tangential mode is

$$p = - p_0 A J_1 \left(\frac{2\pi f_{0,1}}{a} r \right) \cos \theta \, e^{-i2\pi f_{0,1} \tau} \tag{B3}$$

which may be written as

$$p = - p_0 A J_1 \left(\frac{2\pi f}{a} r \right) \cos \theta \, [\cos (2\pi f \tau) - i \sin (2\pi f \tau)] \tag{B4}$$

Using the real part

$$p = - p_0 A J_1 \left(\frac{2\pi f}{a} r \right) \cos \theta \cos (2\pi f \tau) \tag{B5}$$

at the pressure antinode, where $\theta = 0$ and $r = R$, and noting that $f = 0.293 \, a/R$ give

$$\frac{\sqrt{2} \sqrt{p_R^2}}{p_0} = A J_1 (0.5861 \pi) \tag{B6}$$

so that

$$A = 2.43 \frac{\sqrt{p_R^2}}{p_0} \tag{B7}$$

Substituting equation (B7) into (B5) gives

$$p = -2.43 \sqrt{p_R^2} \, J_1\left(1.841 \frac{r}{R}\right) \cos(2\pi f \tau) \cos\theta \tag{B8}$$

from which

$$\frac{\sqrt{p^2}}{p_0} = 1.718 \frac{\sqrt{p_R^2}}{p_0} \, J_1\left(1.841 \frac{r}{R}\right) \cos\theta \tag{B9}$$

Tangential Particle Velocity

For the magnitudes of pressure fluctuations considered herein, the particle velocity is related to the pressure fluctuation by the acoustic relation given in reference 6 (p. 295):

$$v = \frac{g}{i2\pi f \rho} \, \text{grad}\,(p) \tag{B10}$$

The tangential component v_θ is obtained from equation (B10):

$$v_\theta = \frac{g}{i2\pi f r\rho} \frac{\partial p}{\partial\theta} \tag{B11}$$

Substituting equation (B7) into equation (B4) results in

$$p = -2.43 \sqrt{p_R^2} \, J_1\left(1.841 \frac{r}{R}\right) \cos\theta \, [\cos(2\pi f\tau) - i\sin(2\pi f\tau)] \tag{B12}$$

By noting that $f = 0.293\, a/R$ and $g(a\rho) = a/(rp_0)$ the following equation is obtained:

$$v_\theta = 1.32 \frac{a}{r} \frac{\sqrt{p_R^2}}{p_0} \frac{R}{r} J_1\left(1.841 \frac{r}{R}\right) \sin\theta \, [-i\cos(2\pi f\tau) - \sin(2\pi f\tau)] \tag{B13}$$

4379

Using the real part results in

$$v_\theta = -1.32 \frac{a}{\gamma} \frac{\sqrt{p_R^2}}{p_0} \frac{R}{r} J_1\left(1.841 \frac{r}{R}\right) \sin\theta \sin\left(2\pi f \tau\right) \qquad (B14)$$

In terms of root-mean-square particle velocity, equation (B14) becomes

$$\sqrt{v_\theta^2} = 0.9335 \frac{a}{\gamma} \frac{\sqrt{p_R^2}}{p_0} \frac{R}{r} J_1\left(1.841 \frac{r}{R}\right) \sin\theta \qquad (B15)$$

In the limit at $r = 0$ and along $\theta = \pi/2$, equation (B15) becomes

$$\sqrt{v_\theta^2} = 0.859 \frac{a}{\gamma} \frac{\sqrt{p_R^2}}{p_0} \qquad (B16)$$

Radial Particle Velocity

From equation (B10) the radial particle velocity component is

$$v_r = \frac{g}{i2\pi f \rho} \frac{\partial p}{\partial r} \qquad (B17)$$

Noting that $f = 0.293\, a/R$ and $g/a\rho = a/\gamma p_0$ and using equation (B12) result in

$$v_r = -\frac{1.215a}{\gamma} \frac{\sqrt{p_R^2}}{p_0} \left[J_0\left(1.841 \frac{r}{R}\right) - J_2\left(1.841 \frac{r}{R}\right) \right] \cos\theta \left[-i \cos\left(2\pi f \tau\right) - \right.$$

$$\sin\left(2\pi f \tau\right)] \qquad (B18)$$

Using the real part gives

$$v_r = \frac{1.215a}{\gamma} \frac{\sqrt{p_R^2}}{p_0} \left[J_0\left(1.841 \frac{r}{R}\right) - J_2\left(1.841 \frac{r}{R}\right) \right] \cos\theta \sin\left(2\pi f \tau\right) \qquad (B19)$$

In terms of the root-mean-square particle velocity the equation is

$$\sqrt{v_r^2} = 0.859 \frac{a}{\gamma} \frac{\sqrt{p_R^2}}{p_0} \left[J_0\left(1.841 \frac{r}{R}\right) - J_2\left(1.841 \frac{r}{R}\right) \right] \cos\theta \qquad (B20)$$

and at $r = 0$ along $\theta = 0$ it becomes

$$\sqrt{\overline{v_r^2}} = 0.859 \frac{a}{\gamma} \frac{\sqrt{\overline{p_R^2}}}{p_0} \tag{B21}$$

Pressure Fluctuations Experienced by Mixing Wake with

Injection on Duct Axis

To augment the discussion of results, it is of interest to describe the pressure fluctuations encountered by the mixing wake during its transverse motion. The pressure fluctuation experienced by the wake center can be expressed by using the wake displacement y in place of the radius r in equation (B8):

$$p = -2.43 \sqrt{\overline{p_R^2}} \, J_1\left(1.841 \frac{y}{R}\right) \cos (2\pi f \tau) \tag{B22}$$

By noting that the particle velocity near the duct axis is approximately given by equation (4), equation (9) may be written:

$$y = \frac{0.859 \sqrt{2}a}{\pi f \gamma} \frac{\sqrt{\overline{p_R^2}}}{p_0} \sin\left(\frac{\pi f X}{U}\right) \sin\left(2\pi f \tau - \frac{\pi f X}{U}\right) \tag{B23}$$

Substituting equation (B23) into (B22) and noting that $f = 0.293 \, a/R$ give

$$p = -2.43 \sqrt{\overline{p_R^2}} \, J_1\left[\frac{2.43}{\gamma} \frac{\sqrt{\overline{p_R^2}}}{p_0} \sin\left(\frac{\pi f X}{U}\right) \sin\left(2\pi f \tau - \frac{\pi f X}{U}\right)\right] \cos (2\pi f \tau) \tag{B24}$$

Expanding the Bessel function in its infinite series and noting that its argument $1.841 \, y/R$ is small (see eq. (11)) so that the higher-order terms may be neglected give

$$p = -1.215 \sqrt{\overline{p_R^2}} \left[\frac{2.43}{\gamma} \frac{\sqrt{\overline{p_R^2}}}{p_0} \sin\left(\frac{\pi f X}{U}\right) \sin\left(2\pi f \tau - \frac{\pi f X}{U}\right)\right] \cos (2\pi f \tau) \tag{B25}$$

Normalizing gives the following equation:

$$\frac{\gamma p_O p}{\overline{p_R^2}} = -2.95 \sin\left(\frac{\pi f X}{U}\right) \sin\left(2\pi f \tau - \frac{\pi f X}{U}\right) \cos\left(2\pi f \tau\right) \qquad \text{(B26)}$$

At antinodal stations, $f X/U = 0.5, 1.5, \ldots$ and equation (B26) becomes

$$\frac{\gamma p_O p}{\overline{p_R^2}} = 2.95 \cos^2\left(2\pi f \tau\right) \qquad \text{(B27)}$$

REFERENCES

1. Truman, John C., and Newton, Roger T.: Why Do High-Thrust Engines Screech? Aviation Age, vol. 23, no. 5, May 1955, pp. 136-143.

2. Blackshear, Perry L., Rayle, Warren D., and Tower, Leonard K.: Study of Screeching Combustion in a 6-Inch Simulated Afterburner. NACA TN 3567, 1955.

3. Berman, Kurt, and Logan, Stanley E.: Combustion Studies with a Rocket Motor Having a Full-Length Observation Window. Jour. Am. Rocket Soc., vol. 22, no. 2, Mar.-Apr. 1952, pp. 78-85.

4. Smith, R. P., and Sprenger, D. F.: Combustion Instability in Solid-Propellant Rockets. Fourth Symposium (International) on Combustion, The Williams & Wilkins Co., 1953, pp. 893-906.

5. Mickelsen, William R., and Baldwin, Lionel V.: Aerodynamic Mixing Downstream from Line Source of Heat in High-Intensity Sound Field. NACA TN 3760, 1956.

6. Morse, Philip M.: Vibration and Sound. Second ed., McGraw-Hill Book Co., Inc., 1948.

7. Moore, Franklin K., and Maslen, Stephen H.: Transverse Oscillations in a Cylindrical Combustion Chamber. NACA TN 3152, 1954.

8. Mickelsen, William R.: An Experimental Comparison of the Lagrangian and Eulerian Correlation Coefficients in Homogeneous Isotropic Turbulence. NACA TN 3570, 1955.

9. Crocco, Luigi, and Cheng, Sin-I: Theory of Combustion Instability in Liquid Propellant Rocket Motors. Agardograph No. 8, Butterworths Sci. Pub., 1956.

10. Rogers, Don E., and Marble, Frank E.: A Mechanism for High-Frequency
       Oscillation in Ramjet Combustors and Afterburners. Jet Prop.,
       vol. 26, no. 6, June 1956, pp. 456-462.

4379
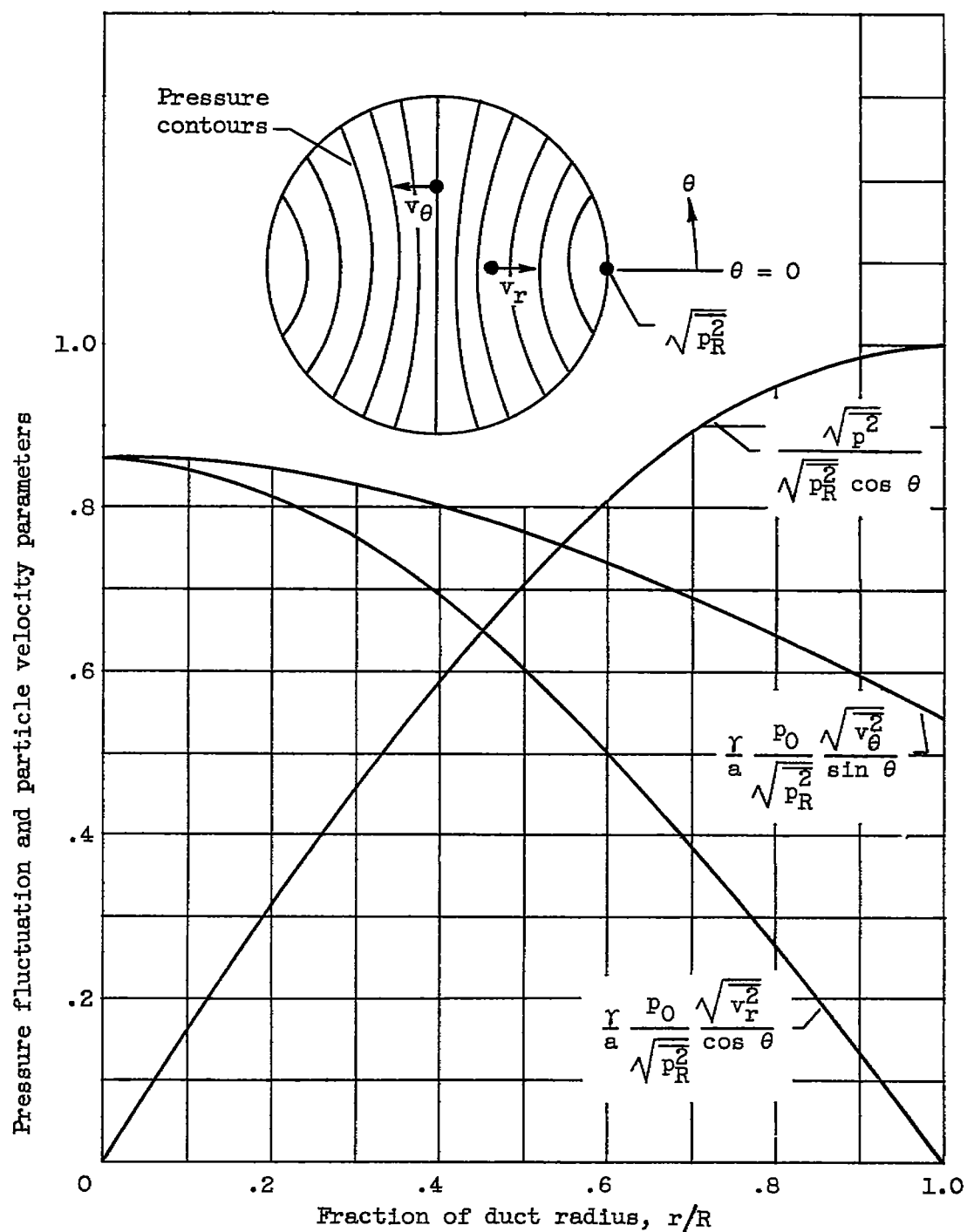
Figure 1. - Pressure fluctuation and particle velocity profiles along specific radii in first pure-standing tangential mode.
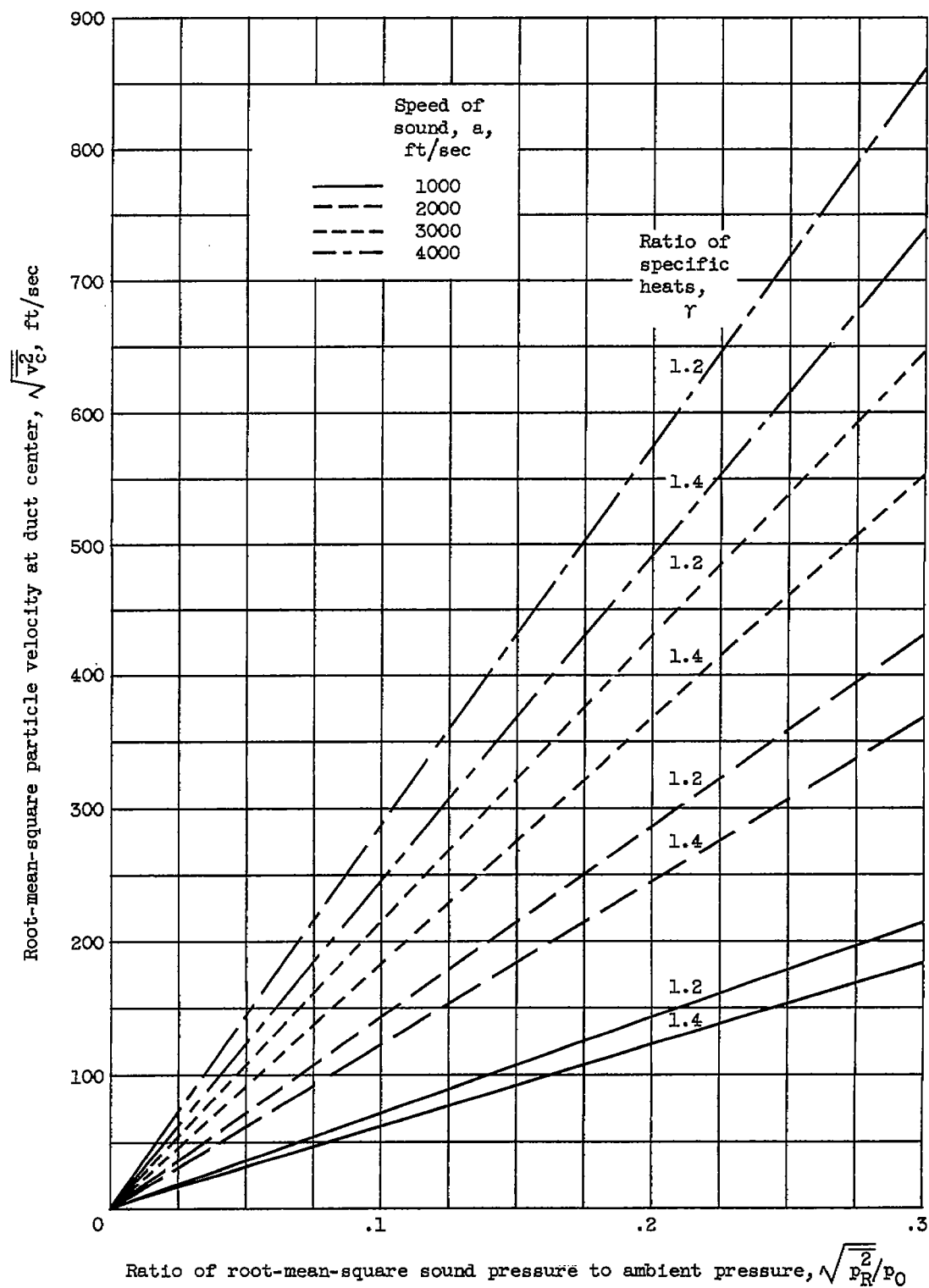
Figure 2. - Relation between particle velocity at duct axis and sound pressure
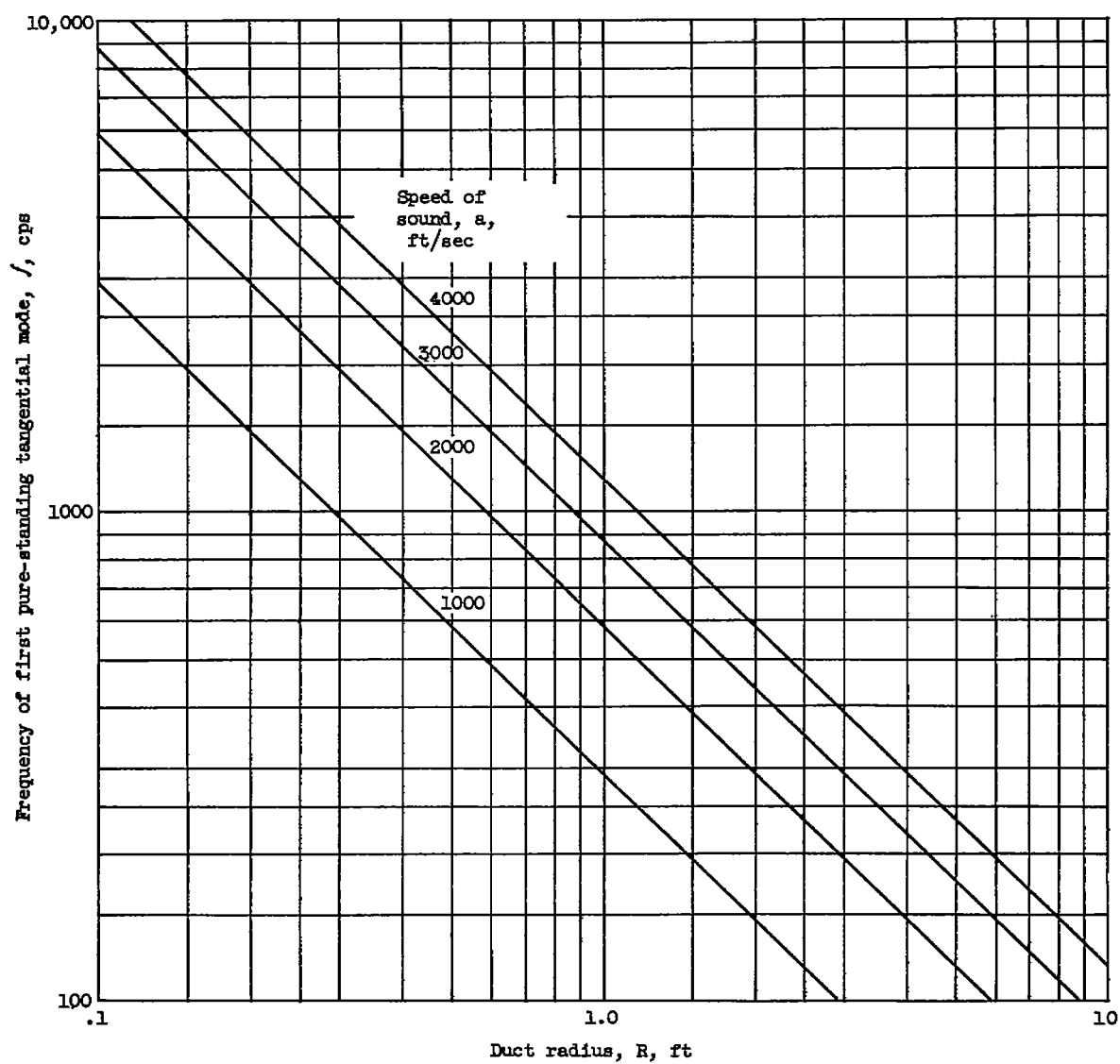in first pure-standing tangential mode.

Figure 3. - Oscillation frequency of first pure-standing tangential mode.
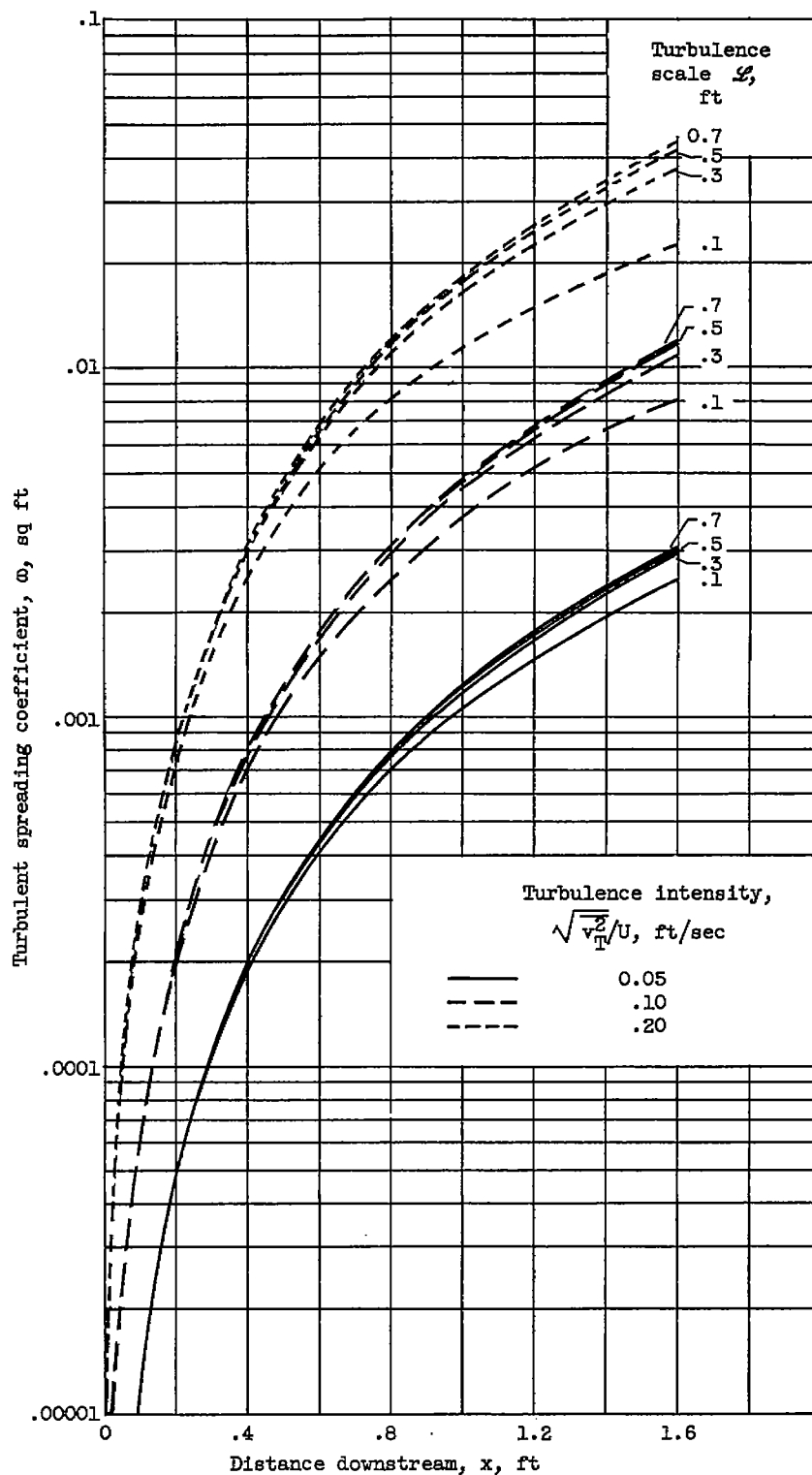
Figure 4. - Turbulent spreading coefficient for range of
turbulence intensities and scales.
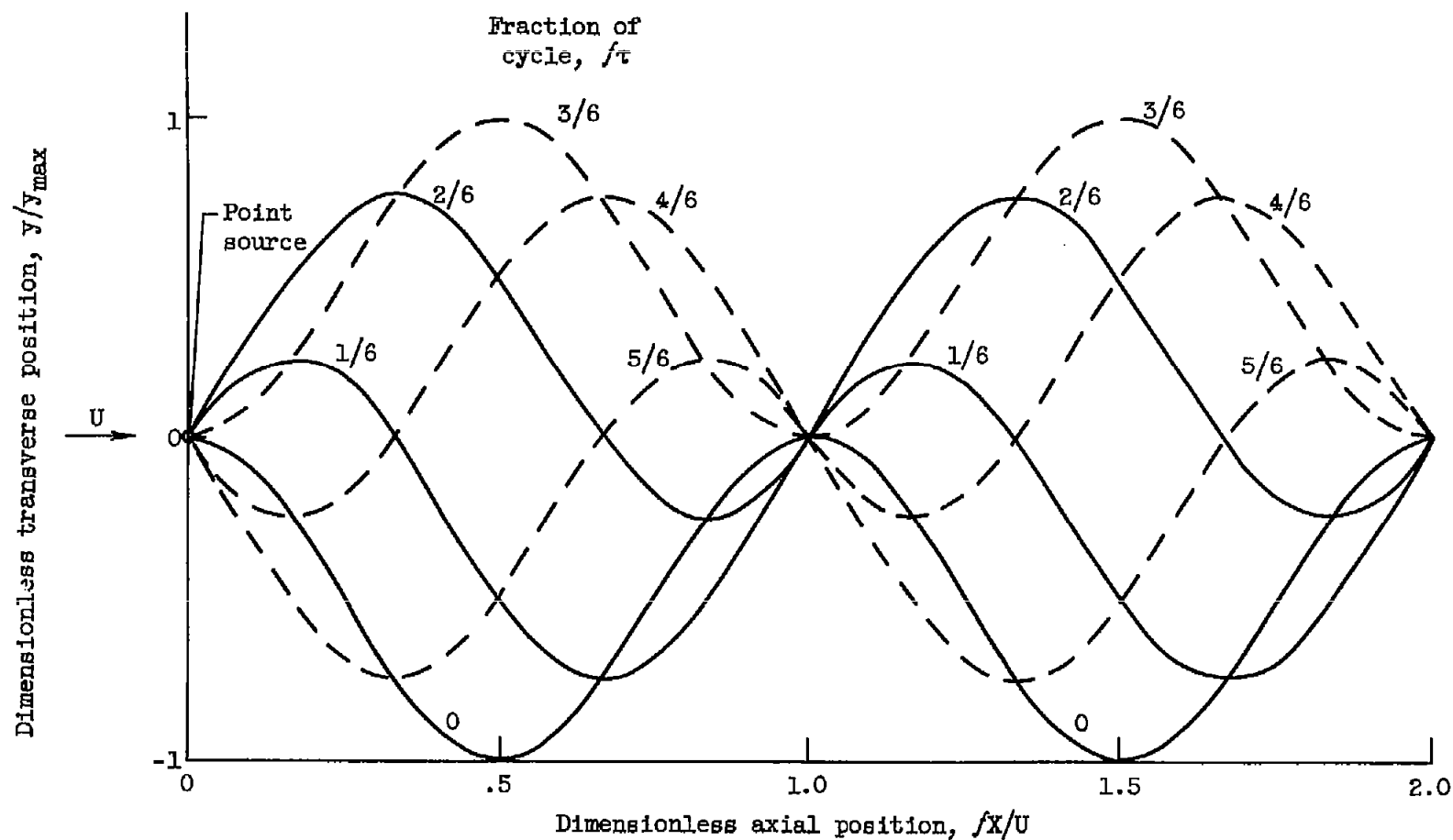
(a) Position of concentration wake center at various times through one cycle.

Figure 5. - Motion of concentration wake with point source on duct axis in first pure-standing tangential mode.
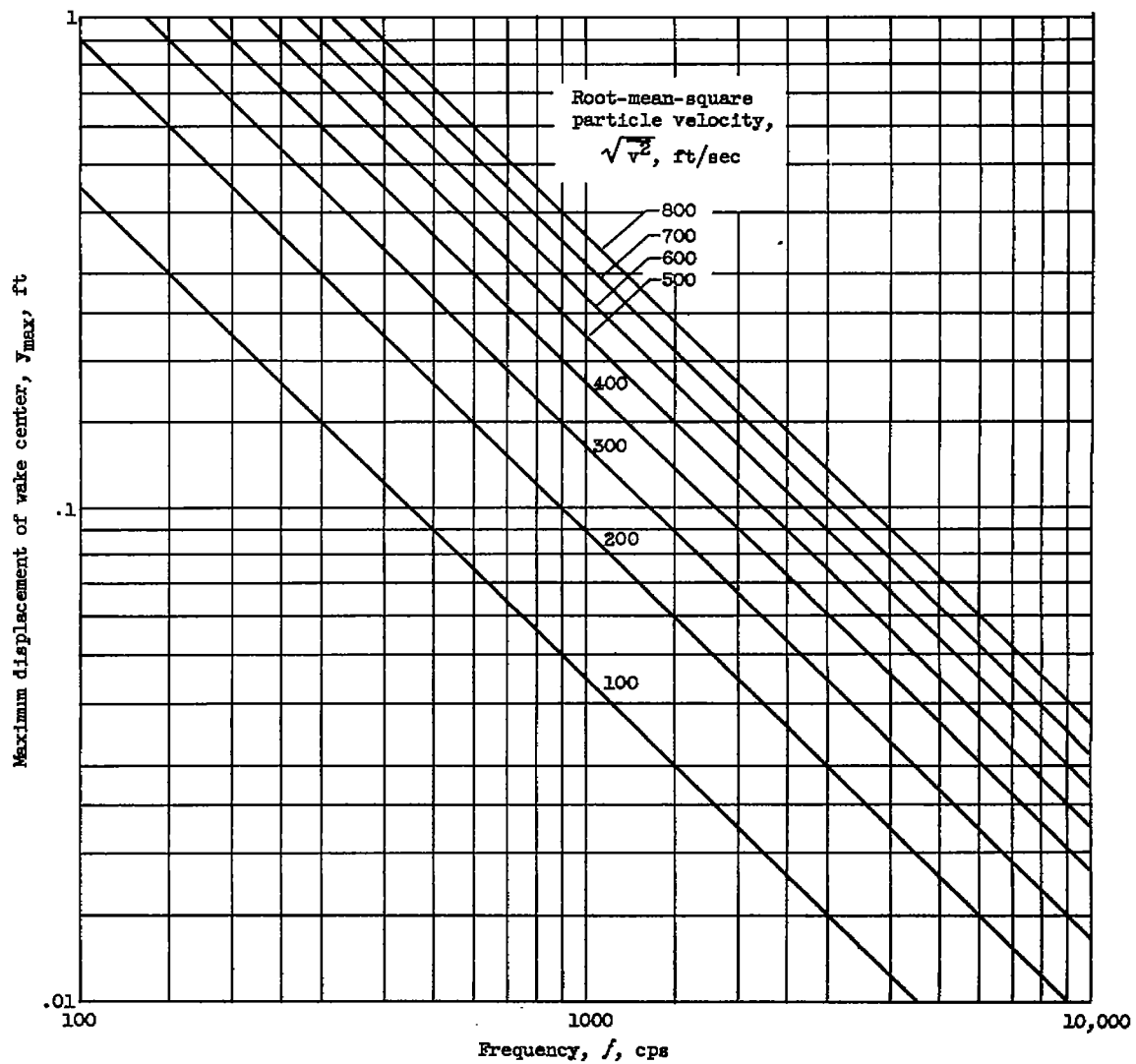
(b) Maximum mixing wake displacement.

Figure 5. - Concluded. Motion of concentration wake with point source on duct axis in first pure-standing tangential mode.
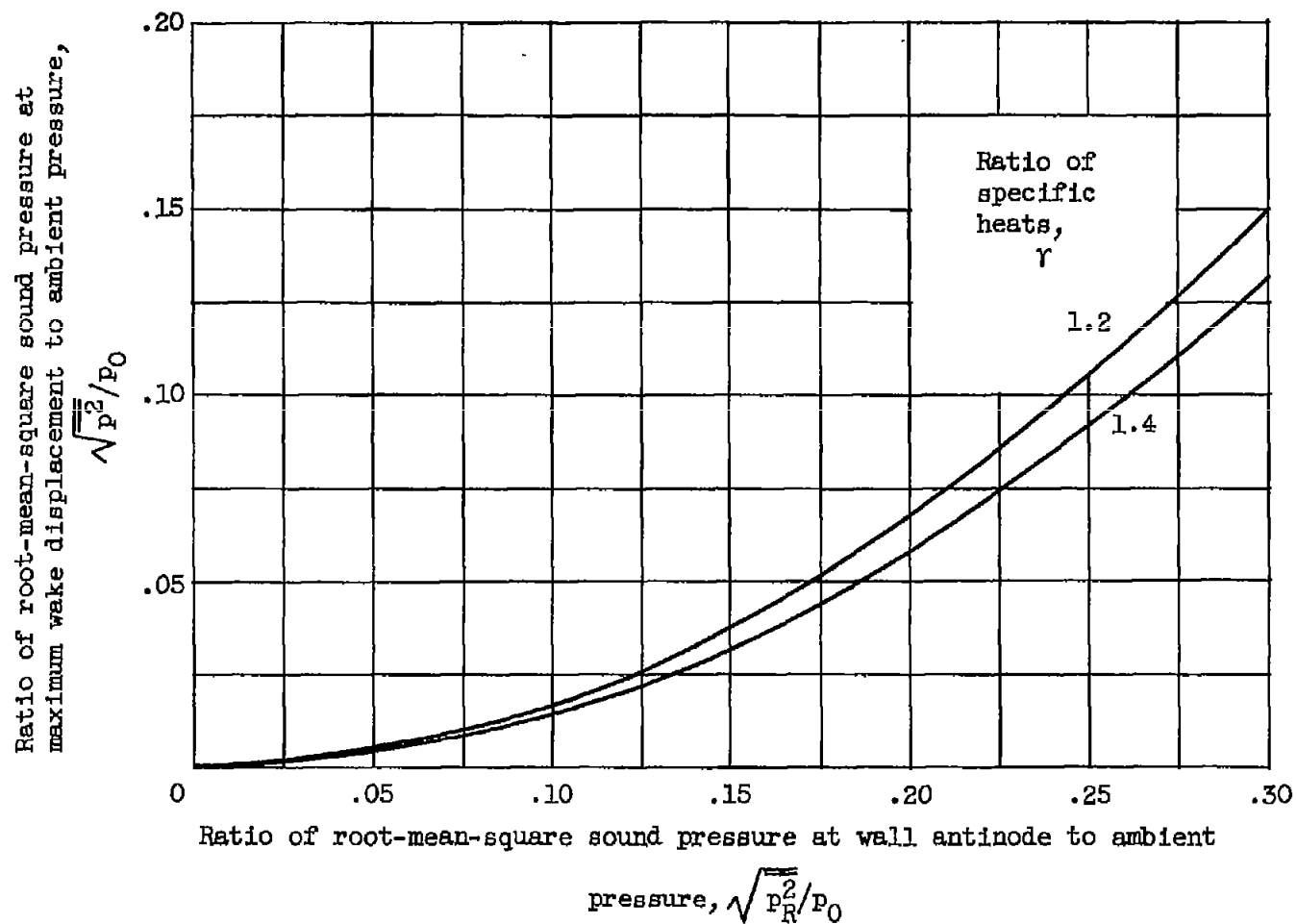
Figure 6. - Acoustic pressure fluctuations at maximum mixing wake displacement for injection at duct centerline in first pure-standing tangential mode.

(a) $\dfrac{1.32}{\gamma} \dfrac{\sqrt{\overline{p_R^2}}}{p_0} = 0.3.$

(b) $\dfrac{1.32}{\gamma} \dfrac{\sqrt{\overline{p_R^2}}}{p_0} = 0.2.$
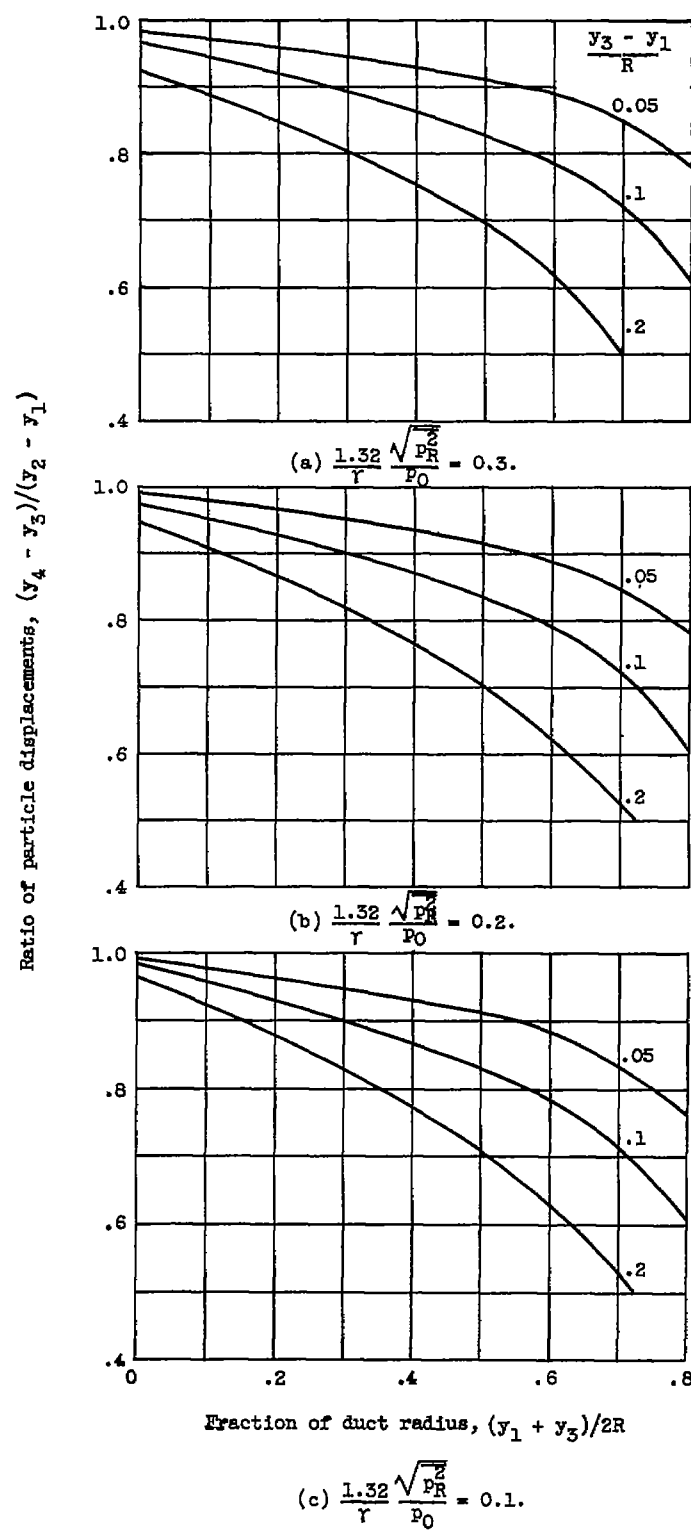
(c) $\dfrac{1.32}{\gamma} \dfrac{\sqrt{\overline{p_R^2}}}{p_0} = 0.1.$

Figure 7. - Effect of acoustic pressure field on particle motion.

4379

CS-6

Fuel-oxidant ratio parameter, $\left[p_0(f/A)\right]/w_f$

Profile at wake
position -

———————— Along injection axis

— — — — Nearest duct wall

– – – – Nearest duct axis
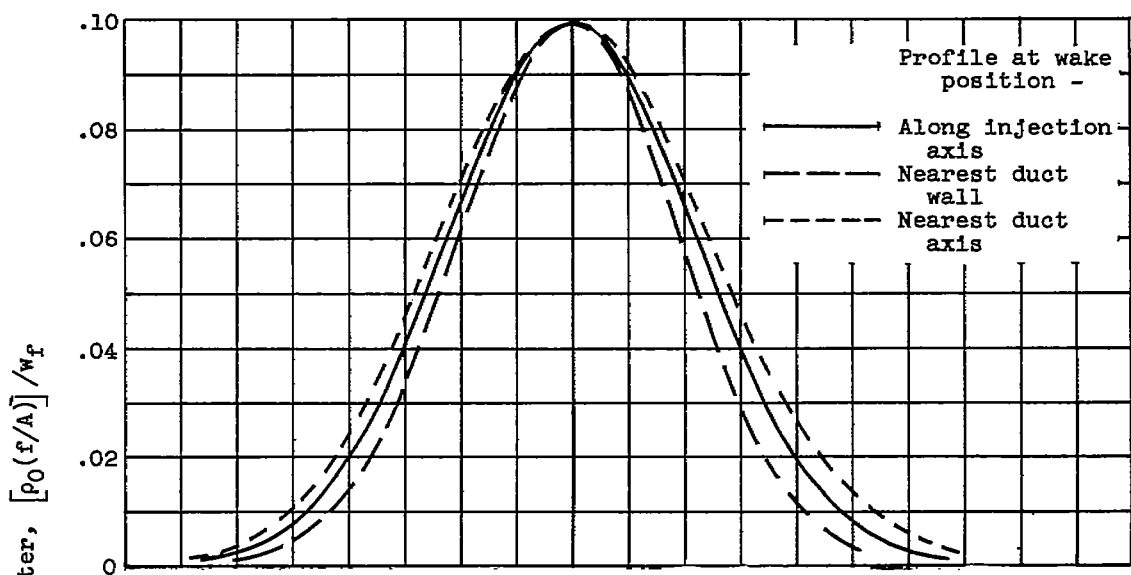
(a) Injection axis at $y_1/R = 0.3$, $R = 1$ foot, $\omega = 3.96 \times 10^{-4}$ square foot, and $\dfrac{1.32}{\gamma} \dfrac{\sqrt{\overline{p_R^2}}}{p_0} = 0.15$.

Incremental fraction of duct radius, $\Delta y/R$
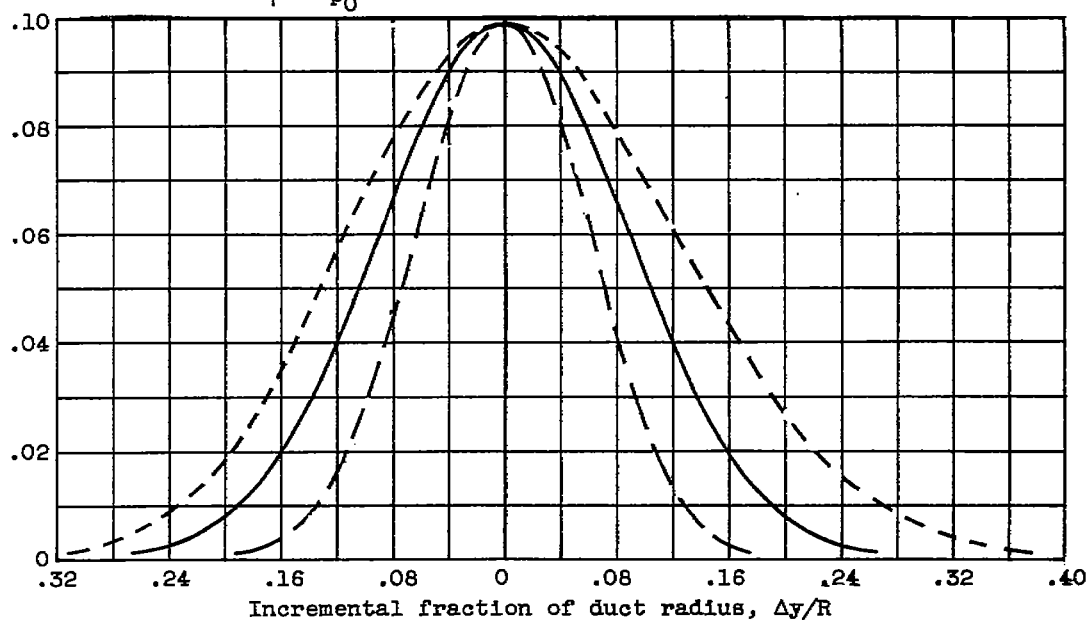
(b) Injection axis at $y_1/R = 0.5$, $R = 1$ foot, $\omega = 3.96 \times 10^{-4}$ square foot, and $\dfrac{1.32}{\gamma} \dfrac{\sqrt{\overline{p_R^2}}}{p_0} = 0.30$.

Figure 8. - Effect of acoustic pressure field on fuel-oxidant ratio profiles with offcenter injection.

(a) Fraction of cycle, 0.5.
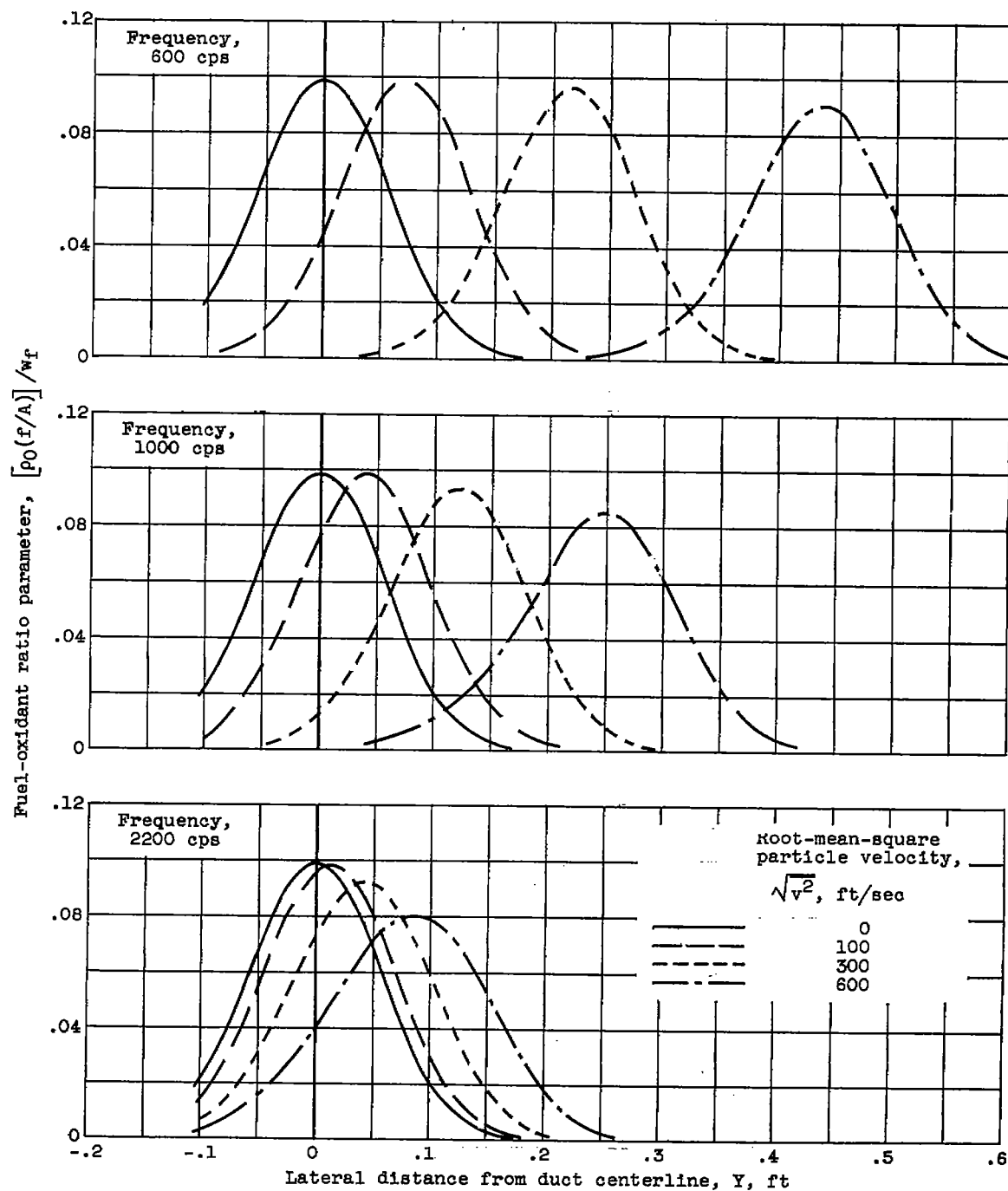
Figure 9. - Effect of oscillation frequency on mixing in first pure-standing tangential mode. Stream velocity, 500 feet per second; turbulence intensity, 5 percent; turbulence scale, 0.1 foot; axial station, 1.25 feet.
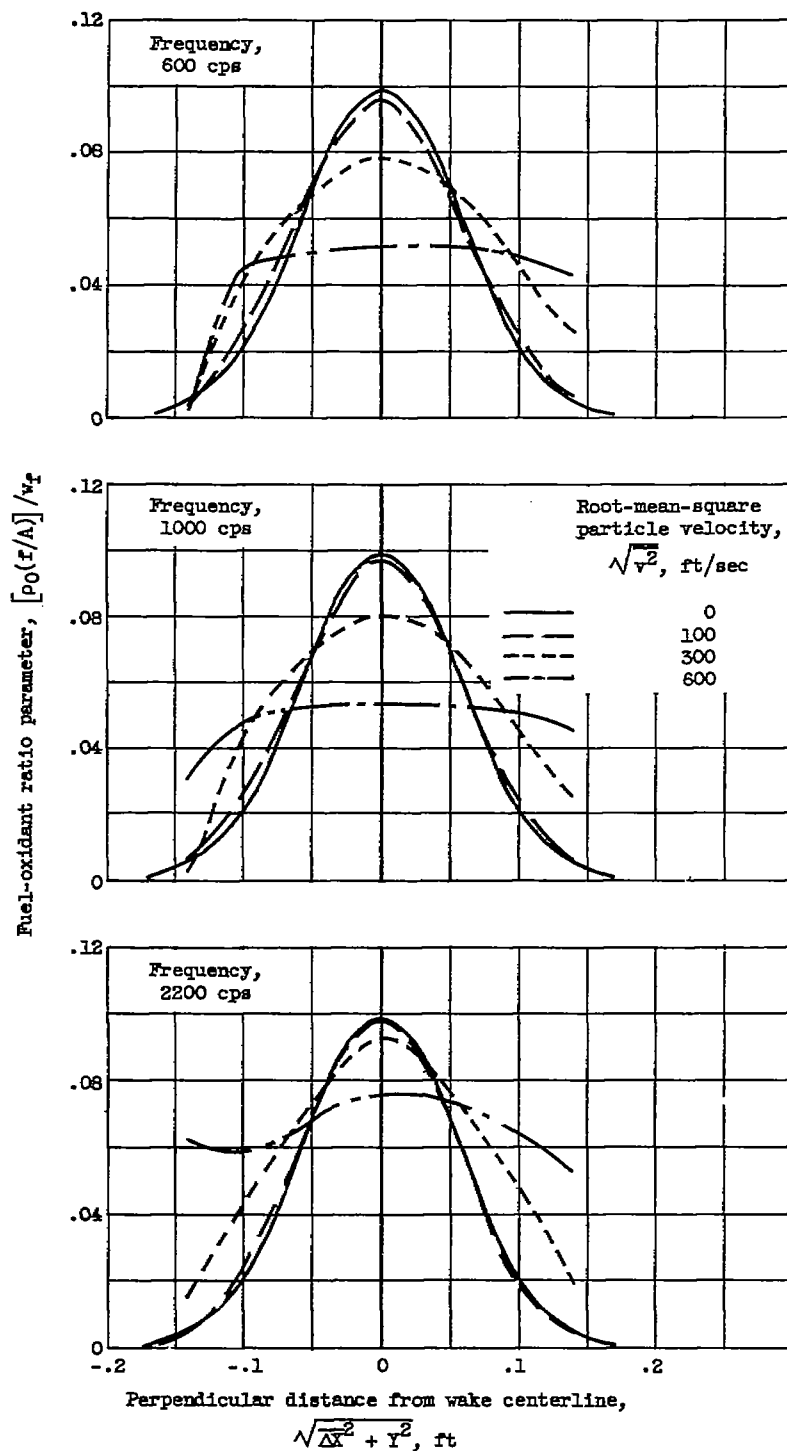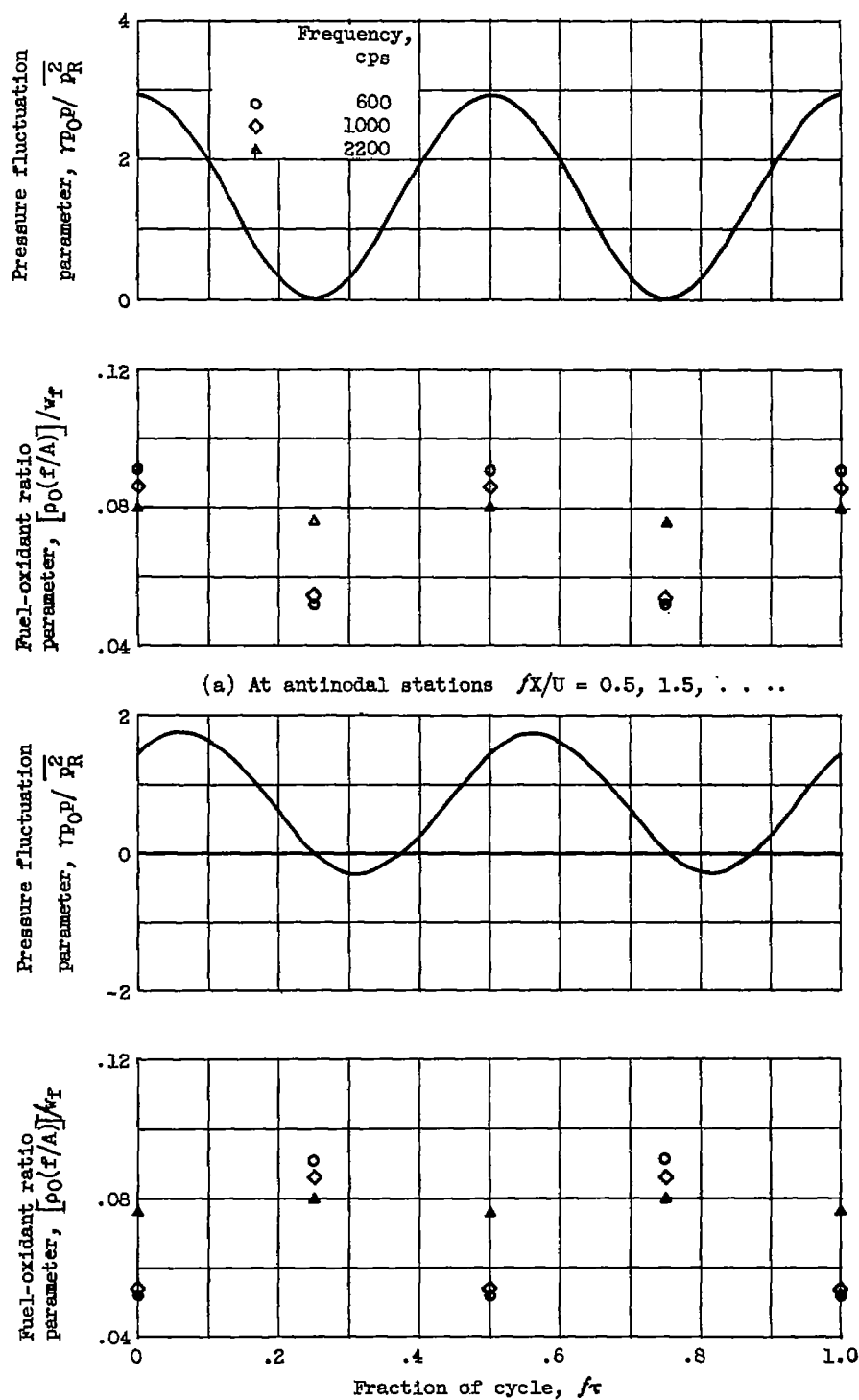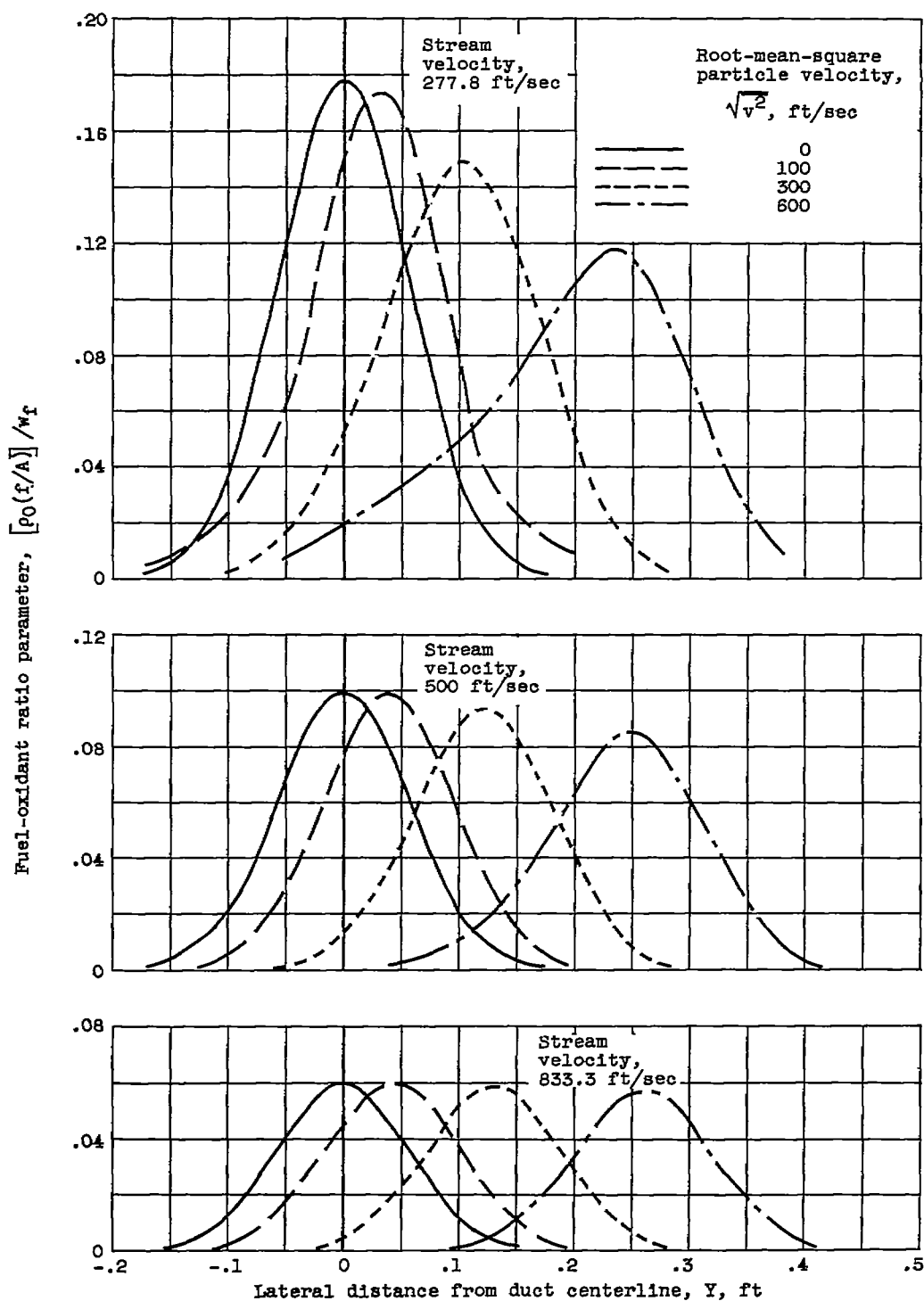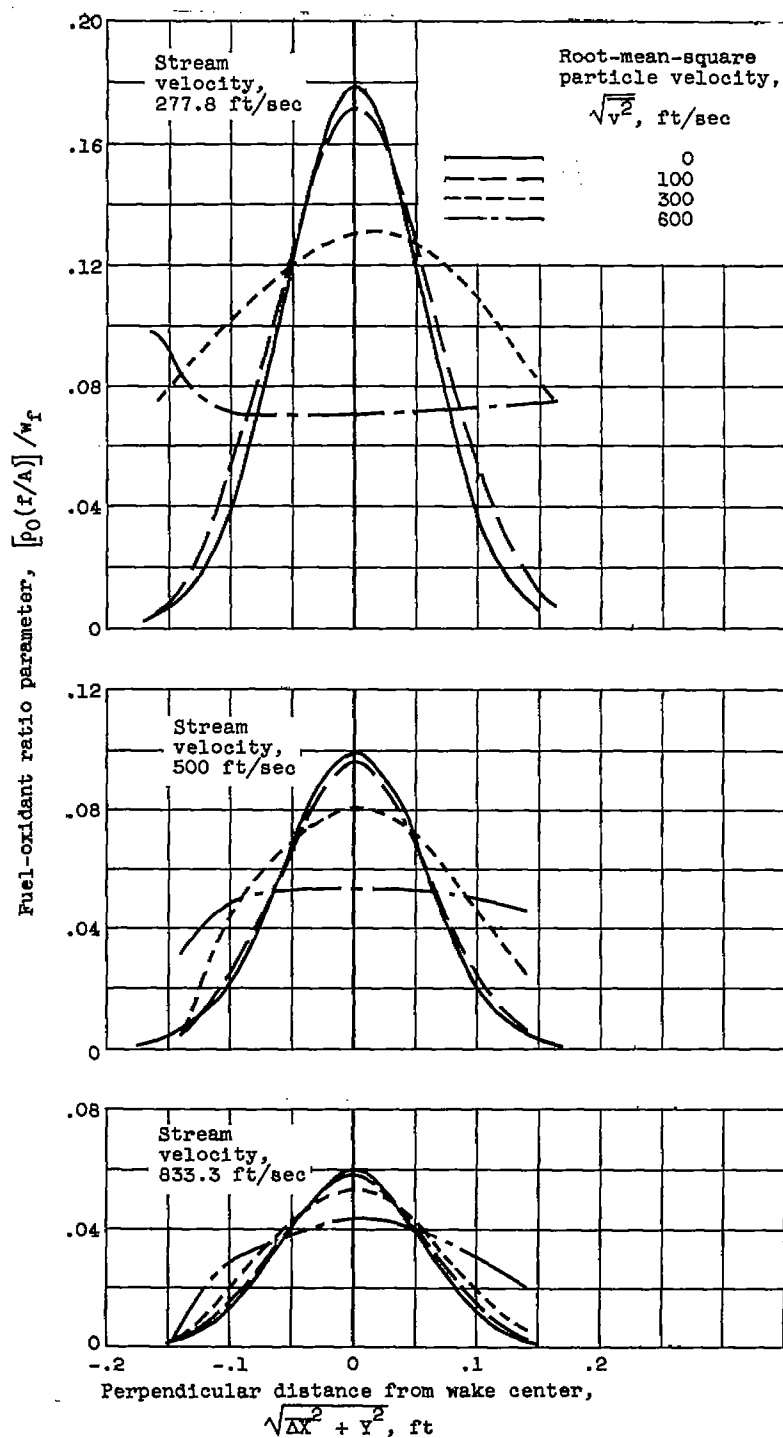
(b) Fraction of cycle, 0.75.

Figure 9. - Concluded. Effect of oscillation frequency on mixing in first pure-standing tangential mode. Stream velocity, 500 feet per second; turbulence intensity, 5 percent; turbulence scale, 0.1 foot; axial station, 1.25 feet.

(a) At antinodal stations fX/U = 0.5, 1.5, ...

(b) At stations fX/U = 0.75, 1.75, ...

Figure 10. - Time-phase relation between pressure and fuel-oxidant fluctuations on the wake center during its transverse motion.

(a) Fraction of cycle, 0.5.

Figure 11. - Effect of stream velocity on mixing in first pure-standing tangential mode. Oscillation frequency, 1000 cycles per second; turbulence intensity, 5 percent; turbulence scale, 0.1 foot; axial station, 1.25 feet.
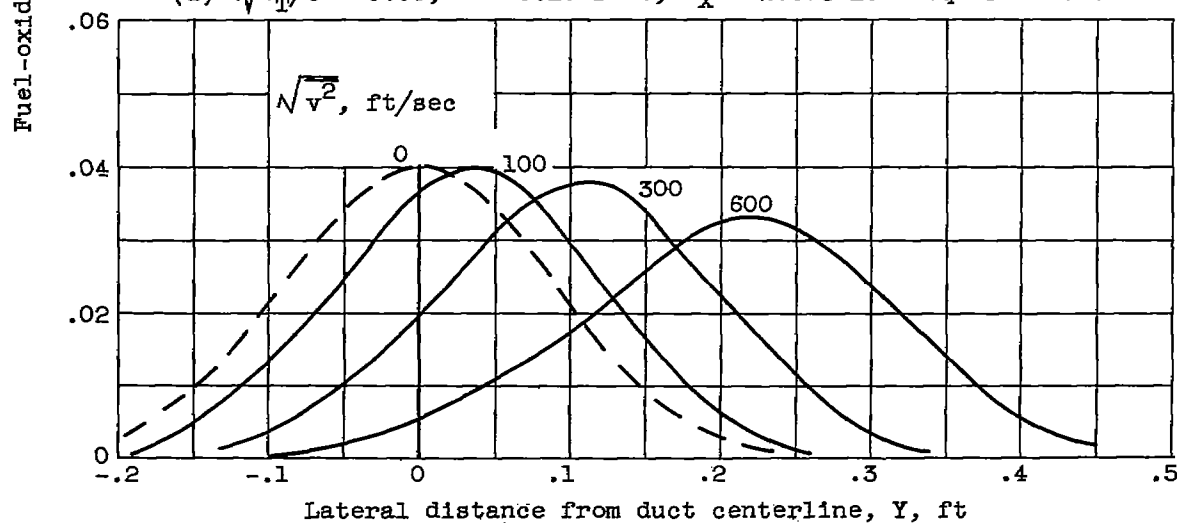
(b) Fraction of cycle, 0.75.

Figure 11. - Concluded. Effect of stream velocity on mixing in first pure-standing tangential mode. Oscillation frequency, 1000 cycles per second; turbulence intensity, 5 percent; turbulence scale, 0.1 foot; axial station, 1.25 feet.
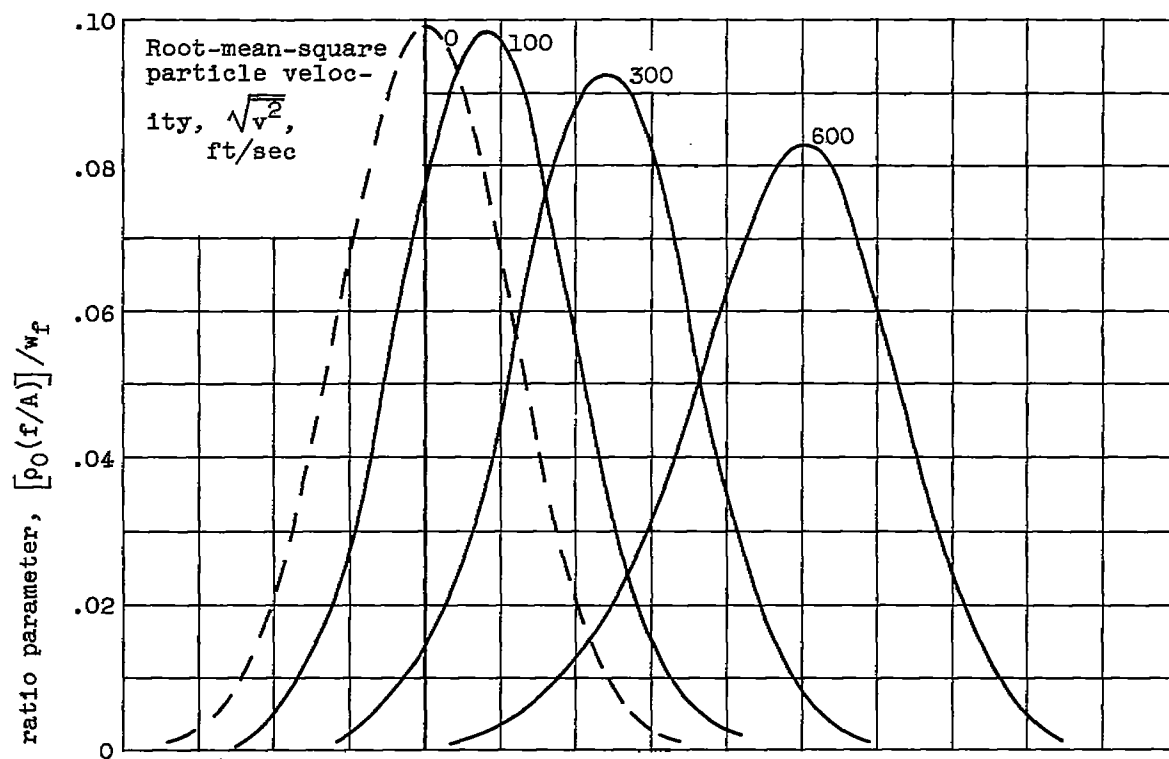
(a) $\sqrt{\overline{v_T^2}}/U = 0.05$; $\mathscr{L} = 0.10$ foot; $\omega_X = 1.603 \times 10^{-3}$ square foot.

(b) $\sqrt{\overline{v_T^2}}/U = 0.10$, $\mathscr{L} = 0.05$ foot, $\omega_X = 3.955 \times 10^{-3}$ square foot.

Figure 12. - Effect of turbulence on mixing in first pure-standing tangential mode. Oscillation frequency, 1000 cycles per second; stream velocity, 500 feet per second; axial station, 1.25 feet; fraction of cycle, 0.5.
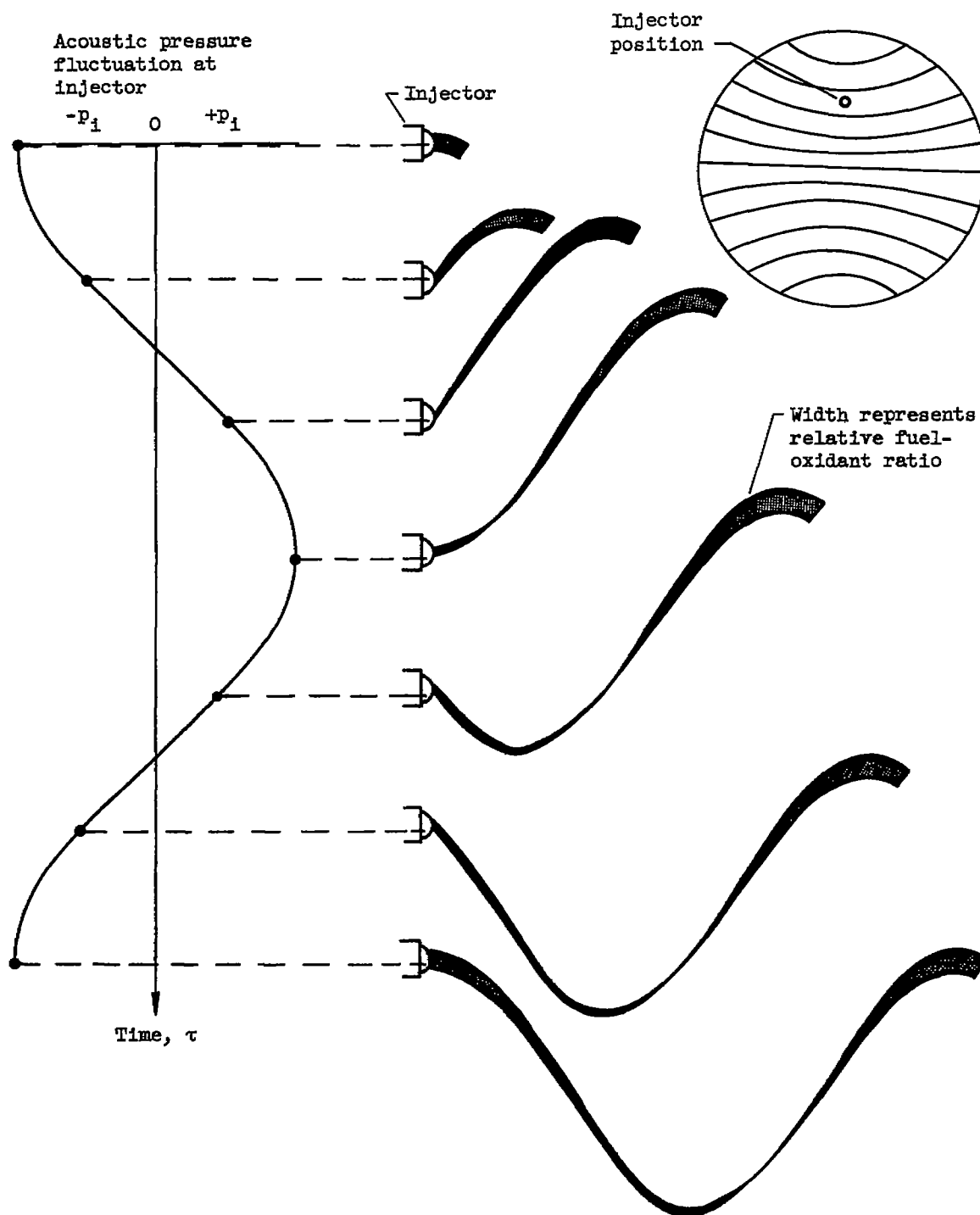
Figure 13. - Mixing in first pure-standing tangential mode with injection at points
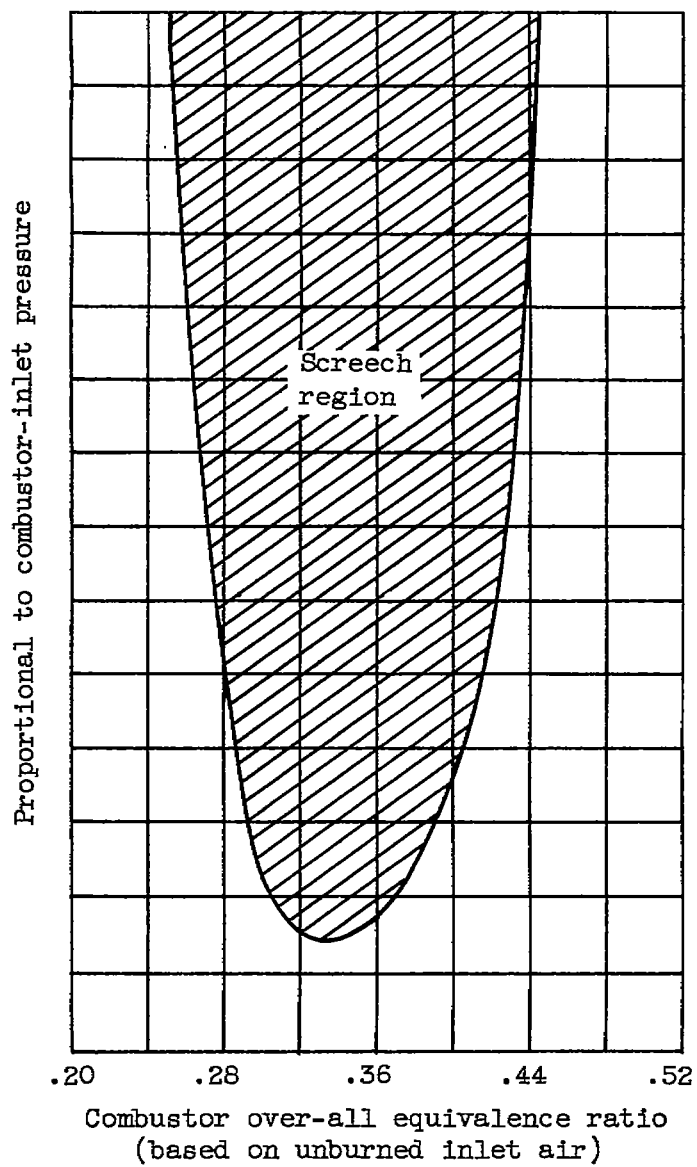away from duct axis.

Figure 14. - Typical combustor screech limits (unpublished data).